Sediment transport processes at the mouth of the Western Scheldt estuary

Master thesis

Author: Sieuwe Stobbelaar

Supervisors: Dr. Maarten van der Vegt & Marco Schrijver

Utrecht University, Faculty of Geosciences, Department of Physical Geography

Rijkswaterstaat, Zee en Delta

Utrecht,

23 July 2023

Abstract

Understanding the sediment transport between the sea and the estuary is crucial for sustainable estuarine management. Sediment fluxes in estuarine environments are controlled by multiple interactive forces like tides, waves, wind, density differences, bathymetry, and trends in sea level rise. Tidal sediment transport is relatively constant while high wave events occur episodically and can transport large amounts of sediment. The sediment transport processes at the mouth of the Scheldt estuary will be studied and the following research questions will be answered: does the sediment transport depend on a) the location in the mouth, b) the position in the vertical and c) the tide, waves and wind?

Measurement frames are used to measure flow velocities and suspended sediment concentration (SSC) at two locations at the mouth of the Western Scheldt estuary, southeast of the Vlakte van de Raan. One measurement site is in a flood channel (F1) and the other in an ebb channel (F3). The measuring frames contained: two Acoustic Doppler Current Profilers (ADCP) & (AQD), two Acoustic Doppler Velocity meters (ADV) and four Optical Backscatter Sensors (OBS).

With these measurements, flow velocity profiles and suspended sediment concentration (SSC) profiles were created over the vertical, to calculate the sediment transported at the two locations. The influence of the waves and tidal currents were studied by calculating the wave and current induced bed shear stresses. To further analyse the influence of the tides, a Godin filter was used to remove the tidal signal from the flow velocities and the SSC, leaving the influences of the tidal asymmetry and the residual currents.

The net sediment transport is landward directed in the flood channel and seaward directed in the ebb channel. The near bed sediment transport is larger in the flood channel than the ebb channel (29032 kg/m vs 18507 kg/m). Most sediment transport occurs during spring tides. The direction and magnitude of the net sediment transport is mainly determined by the tidal component of the sediment transport, being four (F1) and tree (F3) times larger than the residual components. The cause of the direction of tidal sediment transport was the difference in SSC between ebb and flood, caused by peak flow velocity and sediment type differences. The asymmetry of the tides is flood dominant in both locations, and the residual currents are seaward, with larger residual currents at F3. The main driving mechanism of the residual currents is the tidally induced residual flow due to differences in bathymetry.

During the measurement period there were no large wave events, therefore, it is difficult to draw conclusion about the role of large wave events on the net sediment transport. Higher waves did cause higher SSCs, but the resulting increase in sediment transport was only slightly visible in the cumulative sediment transport.

This study presents the main sediment transport processes in ebb and flood channels located in a estuary mouth. Because of the highly dynamic nature of the estuary mouth, projecting these findings to other regions is difficult. Thereby, only part of the sediment transport between the sea and the estuary is solved. But with a better understanding of the sediment transport processes, sediment transport models covering larger areas can be improved.

Contents

1.1 Introduction 1

1.2 General characteristics of the Western Scheldt estuary 1

1.2.1 Morphology 1

1.2.2 Hydrodynamics 2

1.2.3 Sediment balance of the Western Scheldt 3

1.3 Sediment transport processes in the mouth of estuaries 4

1.3.1 Residual sediment transport by tidal asymmetry 4

1.3.2 Residual sediment transport by residual currents 4

1.2.3 Waves and wave-current interaction 6

1.4 Research questions 7

3. Methodology / Method (data and analyses) 8

3.1 Field data and collection 8

3.2 Data analysis 12

3.2.1 velocity profile 12

3.2.2 suspended sediment concentration profile 12

3.2.3 Tide, currents and SSC characteristics 14

3.2.4 Sediment transport and Godin filter 15

3.2.5 Wave and current bed shear stresses 16

4. Results 18

4.1 Tidal characteristics, flow velocity and SSC 18

4.2 Wave and wind characteristics and resulting bed shear stresses. 25

4.3 Sediment transport 28

4.4 Residual flow & residual and tidal sediment transport 31

5. Discussion 39

5.1 Limitations 39

5.2 comparing with other studies. 41

5.3 implications for the two locations as potential sediment storage sites 44

6. Conclusions 44

7. References 45

1.1Introduction

The sediment balance of an estuary is the relation between outflowing and incoming sediment. The sediment balance is positive when the inflow of sediment is larger than the outflow. To keep up with sea level rise, the sediment balance of an estuary must be positive, and the sediment has to be distributed across the estuary to keep the estuary from drowning. Upstream, sediment enters the estuary via a river, and downstream the sediment enters the estuary via the estuary mouth. The upstream river inflow from sediment is relatively well known, while the estuary mouth is a large and complex system with multiple channels and shoals where sediment fluxes are less well understood. Understanding the sediment transport between the sea and the estuary is crucial for sustainable estuarine management.

Sediment transport in the estuary mouth is controlled by multiple interactive forces like tides, waves, wind, density differences, bathymetry, and trends in sea level rise. Tidal residual sediment transport follows the spring neap cycle but is relatively constant, while high wave events occur episodically and can transport large amounts of sediment. Transported sand and mud can originate from fluvial and marine sources (Dalrymple et al., 1992; Schubel & Carter, 1984) and from within the estuary itself.

The aim of this study is to quantitate the sediment transport between sea and the estuary and to find the driving sediment transport processes. To achieve the aim of this thesis, the sediment transport processes at the mouth of the Scheldt estuary will be studied. Section 1.2 describes the general characteristics of the Western Scheldt; section 1.3 describes the different sediment transport processes present in an estuary mouth and in section 1.4 the research questions of this study are presented.

1.2 General characteristics of the Western Scheldt estuary

1.2.1 Morphology

The Scheldt estuary is located in North-West Europe, in both Belgian and Dutch territory (figure 1). The coastal plain estuary is approximately 160 km long and one of the major estuaries of the region. The Dutch part of the estuary is about 60 km long and is called the Western Scheldt. The Scheldt estuary is tide dominated with a meso- to macro-tidal regime, according to the classification of Dyer, (1997). It has a funnel-shaped geometry, with a width of almost 5 km near the mouth (Vlissingen) and 1 km near the Dutch-Belgian border. The width-averaged depth is 15 m at Vlissingen and decreases to 3 m near Gent (Wang et al., 2002). The Western Scheldt is characterized by a multiple channel system. Ebb and flood channels are separated by intertidal shoals and show evasive behaviour (van Veen, 1950). The flood channel is relatively straight, while the ebb channel has a more meandering character. Bars are found at the landward side of flood channels and at the seaward side of ebb channels. Ebb channels are generally deeper than flood channels. Therefore, the ebb channels are mainly used as navigational channels. The channels are generally sandy (Wartel, 1977) while the intertidal flats are muddier (Braat et al., 2017). Due to higher exposure to wave action, shoals closer to the sea are sandier. The estuary and the estuary mouth primarily consist of sand (88-95%) with a median grains size between 150 and 250 µm (Elias et al., 2020; Santermans, 2013).

The mouth of the Western Scheldt contains a large sub-tidal shoal area (Vlakte van de Raan) which is flanked by two channels: the Wielingen, the main entrance channel of the Western Scheldt, in the south, and the Oostgat in the north. The Wielingen, the main channel to the Western Scheldt is not yet divided in an ebb and flood channel. The Vlakte van de Raan forms the southern part of a larger shallow subtidal area located seaward of the estuaries in the southwest Netherlands Delta area (the Voordelta).

1.2.2 Hydrodynamics

The tides in the Western Scheldt are dominantly semi-diurnal. As the tidal wave travels up the estuary, the tidal range amplifies from 3.8 m near the mouth to 5.2 m near Antwerp. The tidal prism is 2 x 10^9 m^3. This causes typical tide-induced discharges during ebb and flood to be 150 times larger than the yearly average river discharge of 100 M^3/s. Based on the ratio between tidal prism and discharge, the estuary can be considered well mixed downstream of Hansweert (Verlaan, 1998). Therefore, the influence of density differences on water level and water movement is small. The maximum depth-averaged current velocities in the channels are in the order of 1–1.5 m/s (Wang et al., 2002).

At the mouth of the Western Scheldt the incoming tidal signal from the North Sea is already asymmetric due to deformation of tide through the North Sea basin. The vertical tide is flood dominant, the duration difference between the falling tide and the rising tide at Vlissingen amounts to half an hour. The duration difference increases upstream, reaching 2 h near Antwerp and almost 4 h near the tidal limit at Gent. The phase difference between vertical and horizontal tide is about 2.5 h (Wang et al., 2002).

On the ebb-tidal delta waves, next to tides, are also a forcing mechanism. The wave climate consists mainly of wind-generated waves in the shallow North Sea. The mean significant wave height of incoming waves is 1.3 m, and the main wave direction is from the west southwest, with a corresponding mean wave period of 5 seconds (Roskam, 1988; Wijnberg et al., 1995). Wind-generated waves occasionally reach heights of over 6 meters during storms, with additional water-level surges of more than 2 m (Elias et al., 2020). The large shallow Vlakte van de Raan shoal shelters the estuary from the North-Sea waves. Therefore, waves in the Western Scheldt are typically 0.5 m or smaller. Wave heights at the mouth of the Western Scheldt differ between locations, depending on the position relative to the Vlakte van de Raan and the local bathymetry.

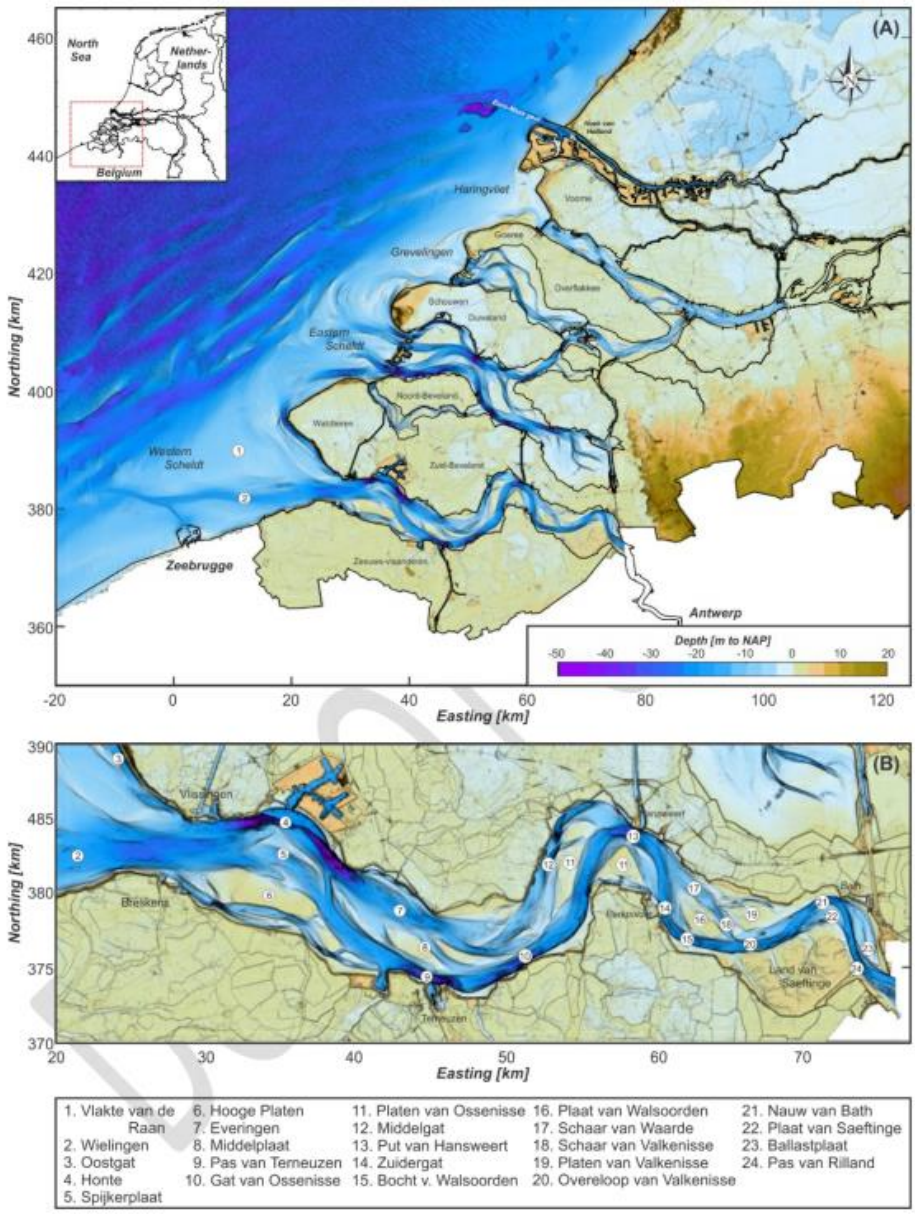

Figure 1: Overview of (A) the estuaries that form the Voordelta, and (B) the main channels and shoals in the Western Scheldt estuary. The underlying DEM is based on 2016-2017 survey data. Depths are given in meters relative to NAP (Normaal Amsterdams Peil), the Dutch ordnance datum which is about present-day mean sea level (Elias et al., 2020).

1.2.3 Sediment balance of the Western Scheldt

Over the 1860 to 1955 period, the Western Scheldt narrowed and deepened, while the estuary imported mud (0.5 to 1.5 million m^3 per year) and exported sand (1.5 to 2.5 million m^3 per year) (Dam et al., 2022). Marine mud is transported through the estuary and can reach the estuarine turbidity maximum which is located near Antwerp (Dam & Cleveringa, 2013). A net seaward sand transport is present in the western part of the Western Scheldt and at Terneuzen a reversal of the sand transport direction is found, and a

net landward sand transport is present in the eastern part of the Western Scheldt (Dam & Cleveringa, 2013).

1.3 Sediment transport processes in the mouth of estuaries

The principal forcing factors of water motion in estuaries are tides, wind, river flow and density-driven circulations. Tidal currents transport large amounts of sediment in and out of an estuary during one tidal cycle, but the net sediment transport is significantly smaller. The net residual transport accounts for less than 10% of the total sediment transport in ebb or flood direction (Shellenbarger et al., 2013). Tidal residual sediment transport follows a spring-neap cycle but apart from that is relatively constant. Storm events on the other hand occur episodically and can transport large amounts of sediment. Both waves and tidal currents are influenced by the bathymetry of the estuary mouth, which consists of ebb- and flood channels and shoals.

Residual sediment transport by tidal asymmetry is explained in section 1.3.1. Section 1.3.2 will discuss residual sediment transport by residual currents and in section 1.3.3 I will discuss sediment transport by wind-driven currents, waves and wave-current interactions. Intertwined through these sections is the bathymetry, and how this effects the sediment transport.

1.3.1 Residual sediment transport by tidal asymmetry

Astronomical ocean tides deform when they propagate into the estuaries because of non-linear processes caused by the estuarine morphology. The tide can be split in horizontal tide and vertical tide. The vertical tide is asymmetric when the flood period differs from the ebb period. The vertical tide is flood dominant if the time from low water to high water is shorter than the time from high water to low water, if the opposite is true, the tide is ebb dominant. A shorter flood period duration implies a higher maximum flood velocity and thereby higher transport rates and vice versa. The horizontal tide contains two types of asymmetries: the first is about the flood and ebb flow velocities and the second is about the slack duration at high and low water. The first horizontal asymmetry is flood dominant when the maximum flood velocity is higher than the maximum ebb velocity, and the second is flood dominant when the high tide slack water is longer than the low tide slack water (Wang et al., 1999). Both cases will cause a net residual transport in flood direction. Higher maximum flow velocities result in residual bedload and suspended-load sediment transport, while the slack water asymmetry results in residual transport of mostly fine suspended sediment due to the relaxation effect of the suspended sediment concentration.

The horizontal tide is closely related to the vertical tide. An asymmetry in the vertical tide will cause an asymmetry in the horizontal tide. However, the relation between the horizontal and vertical tide is non-linear. As a result, the nature (flood- or ebb-dominance) of the horizontal tide and the vertical tide do not necessarily have to be the same (Wang et al., 1999).

1.3.2 Residual sediment transport by residual currents

Residual currents are of great importance because they can give rise to a net sediment flux. Processes and mechanisms influencing the residual flow velocity in an estuary are density-driven circulations, wind, the river discharge and the tidally induced horizontal circulation (Wang et al., 1999). Tidally induced residual flow is very sensitive to bathymetry (Ridderinkhof, 1988a, 1988b, 1989; Zimmerman, 1978, 1981; Zimmerman J T F, 1980). In the relatively shallow parts, the residual flow tends to be in the flood-

direction, while in the deeper parts the residual flow is in ebb-direction(figure 2)(Ridderinkhof, 1988b, 1988a, 1989; Zimmerman, 1978, 1980, 1981).

Li & O'Donnell, (1997) explain this as follows: The residual circulation is a result of competition among several processes. An inward (flood) flux is caused by local nonlinearity, both in the bottom friction and from propagation of the tidal wave of finite amplitude. This inward flux is larger on the shoals and smaller in the channels because the larger non-linearity in the shallow water. The residual inward flow creates a setup (residual surface elevation) of water at the head of the estuary that produces a pressure gradient. This pressure gradient is approximately uniform across the estuary and drives an outward flow that is larger in the channel centre than on the shoals, because friction is smaller in the deeper parts.

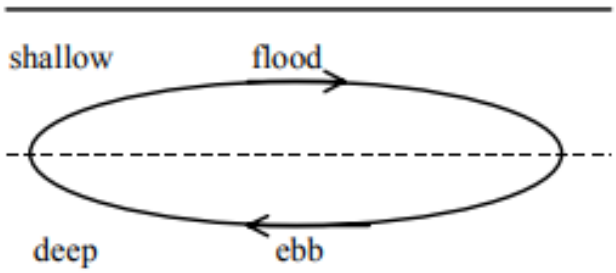

Figure 2: Bathymetry induced circulation (Wang et al., 1999).

When the estuary is bimodal, i.e., with two channels, the residual flow in the deeper channel is usually in ebb direction, while in the shallower channel it is in flood direction (Kjerfve, 1978; van Veen, 1950). The residual currents circulate around the shoals in an estuary and create macro cells as depicted in figure 3 (Bolle et al., 2010; Wang et al., 1999). The intensity of the residual circulations induced by the ebb and flood channels goes through a neap-spring tidal cycle. Furthermore, the direction of the residual flow influences the asymmetry of the maximum flow, i.e., the difference between the maximum ebb and flood flow velocities. The magnitude of the flow velocities is thus influenced by both residual currents and tidal asymmetry.

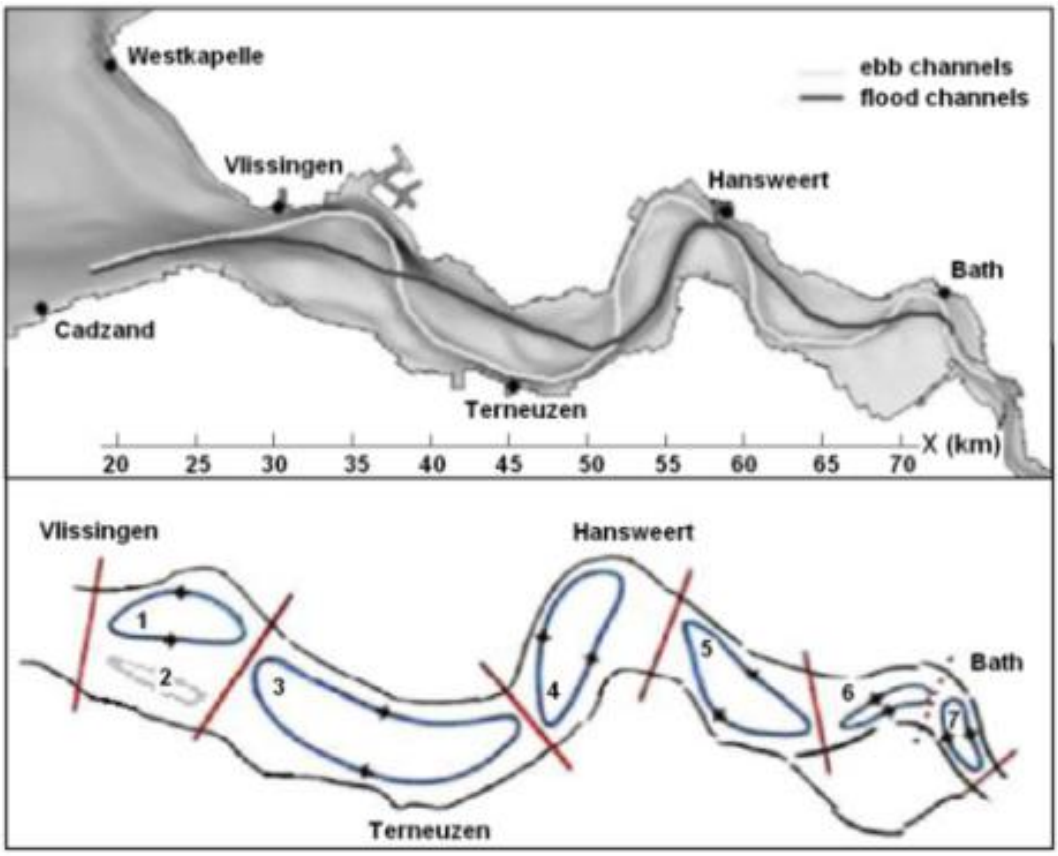

Figure 3: (A) The location of the ebb and flood channels in the Western Scheldt. (B) A schematization of the estuary with macro cells (Bolle et al., 2010).

Wind can in addition to tides be an important forcing in producing residual currents. For both neap and spring tides the wind influences the entire water column, although most of the effect is concentrated at the surface and more often a stronger effect is observed during spring tide due to the occurrence of wind events (Bolaños et al., 2013). The effect of wind on the residual currents is enhanced when the water column is stratified, due to the boundary between layers. In locations with reasonably two dimensional bathymetry, wind can drive surface currents in the direction of the wind, which can create currents in the deeper parts of the estuary in opposite direction, driven by a sea level gradient (Gutiérrez de Velasco & Winant, 2004). When the topography of channels is complicated, the flow direction varies with depth and is not simply related to the local orientation of the bathymetry or the direction of the wind (Gutiérrez de Velasco & Winant, 2004).

1.2.3 Waves and wave-current interaction

Tidal currents are periodic, while waves and wind events occur episodically. Waves can be locally generated by the wind, or they propagate into the basin from the ocean. On the ebb tidal delta, ocean waves are an important factor because they can redistribute sediment. Resuspension of sediment can be caused by wave breaking and by orbital motions under waves. The wave orbital motions induce bed shear stresses on the bed which can bring the sediment into motion and further transport the sediment. High waves with long periods have a higher wave orbital velocity magnitude. Therefore, during storms, there can be an order-of-magnitude increase in suspended-sediment concentration compared to during fair weather (Christie et al., 1999).

The breaking of oblique incident waves generates alongshore currents and can consequently cause alongshore sediment transport. Waves breaking on shoals of an ebb-tidal delta can create a landward flow over the shoals. This occurs for instance at the Tagus estuary mouth, where wave breaking-induced acceleration over the ebb shoal enhances tidal currents during flood, leading to a relative decrease of tidal flow in the deep main channel. During ebb this is reversed (Mengual et al., 2022). Thereby, storm waves can substantially impact the mean circulation at the scale of a wide and deep estuary mouth.

1.4 Research questions

The aim is to quantitate the sediment transport between the North Sea and the Western Scheldt estuary and to find the driving sediment transport processes. To achieve the aim of this thesis, the following research question must be answered:

How does the sediment transport depend on a) the location in the mouth, b) the position in the vertical and c) the tide, waves and wind?

Two common ways of finding the sediment transport in estuaries are models and measurements. Quantifying sediment fluxes in estuaries is mostly done by coupled hydrodynamic, wave and sediment models. These numerical models do not resolve the full morphodynamic behaviour of the system but use flow models and transport formula to compute potential sediment transport (Elias & Hansen, 2013). These models require all relevant processes and dynamics. The input parameter values and process descriptions may include significant uncertainty levels (Diaz et al., 2020) related to for example hydraulic forces like waves and tides and sediment class properties.

Measuring sediment fluxes is a way to validate numerical models but can also be used on itself to quantify sediment transport and find its driving processes. Measuring sediment fluxes requires simultaneous flow and sediment concentration measurements over the vertical and across multiple locations in the estuary or river. These measurements are quite time consuming and costly which is why measurements are mostly used in combination with models. Next to calibrating models, measurements are also used to gain a better understanding of the underlying processes of sediment transport. Model results can cover large areas, while most measurements are more limited to specific locations and specific depths.

There are two common ways of measuring sediment fluxes; stationary and vessel mounted. Both ways have its limitations. Vessel mounted Acoustic Doppler Current Profilers (ADCP) have been used to create a continues vertical current profile along the vessels track. This method gives a good spatial understanding of the differences in currents and sediment concentration but lacks measurements and knowledge of differences over time. Stationary measurements have low spatial resolution but high vertical resolution and are very useful to gain a better understanding of sediment transport at fixed locations because they can collect data over a longer period, but because of the highly dynamic nature of estuaries projecting the findings to other locations is difficult.

Rijkswaterstaat has obtained field data at two contrasting sites at the mouth of the Scheldt estuary. In this study, I will use this data to answer my research questions. Two stationary measurement frames gathered data on hydrodynamics and sediment concentration for a period of about 4 weeks in the summer of 2022. The two measurement frames are located at the mouth of the Scheldt estuary, southeast of the Vlakte van de Raan. One measurement site was in a flood channel and the other in an ebb channel. These two sites are also potential locations of temporal sediment storage or nourishment.

3. Method

3.1 Field data and collection

The data used has been collected by Rijkswaterstaat. Two frames were placed near the Vlakte van de Raan (figure 4) and the instruments have collected data for about one month around June 2022 (see table 1). The field data covers about two neap tides and two spring tides. Frame 1 (F1) is in a flood channel, while Frame 3 (F3) is located in an ebb channel. Figure 5 shows the bathymetry of the study area, the mean water depths at F1 and F3 are 9.7 m and 12.0 m respectively.

Table 1: Global information measuring frames.

	Frame 1	Frame 3
Latitude [° N/S]	51.43594	51.42537
Longitude [° E/W]	3.33453	3.40012
RDX [m]	12282	16809
RDY [m]	384991	383689
Start date	07-06-2022 14:00 MET	07-06-2022 14:30 MET
End date	05-07-2022 10:00 MET	05-07-2022 10:30 MET
Magnetic variation [°]	1.66	1.66

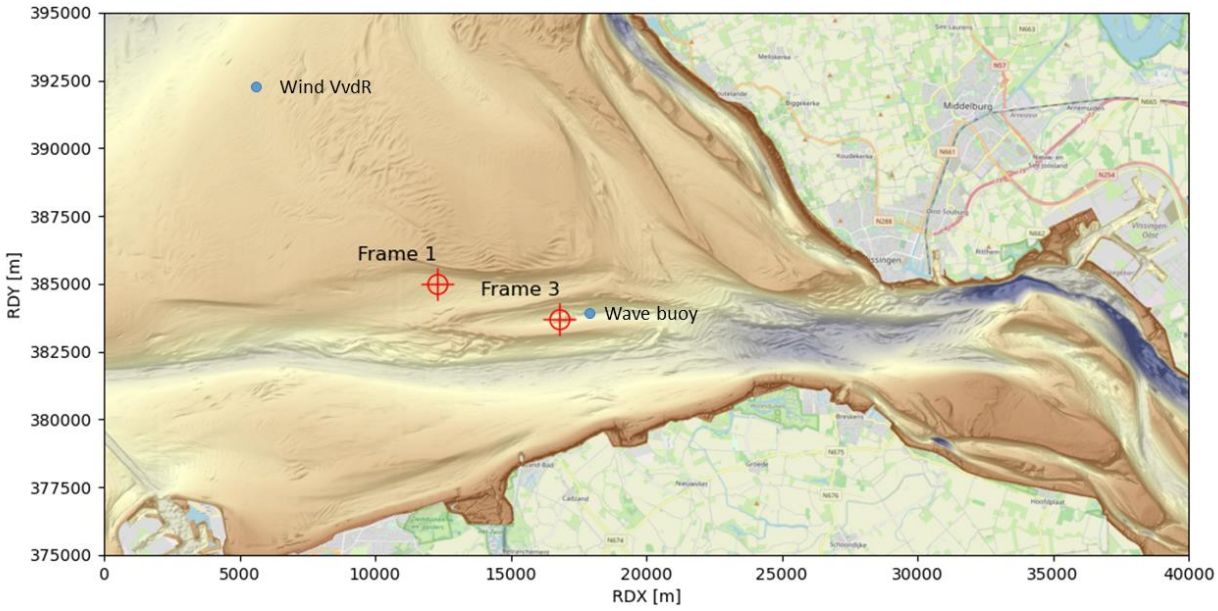

Figure 4 Research location, the red markers are the locations of data frame 1 and 3, the blue dots represent the locations of the wind and wave measurements.

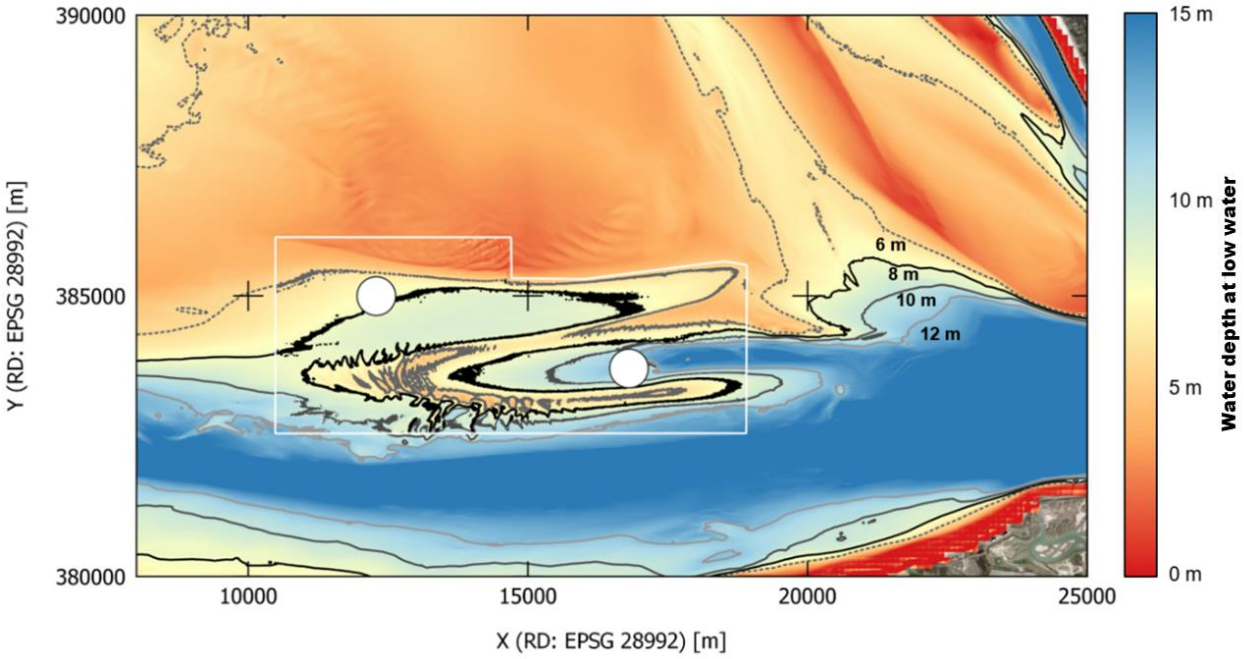

Figure 5: Bathymetry of the study area. The locations of the two frames are represented by the white circles.

The frames contained six different measuring instruments (figure 6); two Acoustic Doppler Current Profilers (ADCP) &(AQD), Two Acoustic Doppler Velocity meters (ADV), four Optical Backscatter Sensors (OBS), a Multi Parameter Probe (MPP) and a 3D Sand Ripple Profiling Logging Sonar (SONAR). The location of the instruments placed on Frames 1 and 3 are almost identical. Table 2 contains all the locations of the instruments on the frames. The ADCP is located at the top of the frame at 2.297 m and is pointed upward. The ADCP measures flow velocities every 0.5 m to create a flow profile and starts measuring 1.06 m from its sensor location. The AQD is placed at around 0.48 m and is pointed towards the bottom. It measures flow velocities every 0.03 m, and the first velocity is measured 0.077 m from the sensor. All four OBS sensors are in the first meter (at about 0.2, 0.3, 0.5 and 0.8 m). The two ADV's are located at around 0.35 and 0.65 m and are pointing down. The ADV's measure the flow velocity at 0.157 m from the probe. The AQD, ADCP and ADV velocity meters sampled at different rates. The AQD is sampled at a rate of 4 Hz, the ADV's at 2 Hz and the ADCP at 0.62 Hz. The OBS sensors samples at a rate of 2 Hz.

On frame 3, the ADV_B velocity meter and the OBS_30 and OBS_20 backscatter sensors stopped measuring about a week earlier than planned on June 27th at 00:00:00.

Table 2: Sensor positions on the frames and their measuring frequency.

FRAME	INSTRUMENT	Z [M]	REFERENCE POINT	FREQUENCY [HZ]
F1	ADCP	2.297	Top centre	0.62
	AQD	0.48	Mid transducer centre	4
	ADV_T	0.645	Mid transducer centre	2
	OBS_80	0.798	Optical centre	2
	OBS_50	0.5	Optical centre	2

	ADV_B	0.346	Mid transducer centre	2
	OBS_30	0.3	Optical centre	2
	OBS_20	0.193	Optical centre	2
F3	ADCP	2.297	Top centre	0.62
	AQD	0.471	Mid transducer centre	4
	ADV_T	0.651	Mid transducer centre	2
	OBS_80	0.792	Optical centre	2
	OBS_50	0.488	Optical centre	2
	ADV_B	0.35	Mid transducer centre	2
	OBS_30	0.301	Optical centre	2
	OBS_20	0.202	Optical centre	2

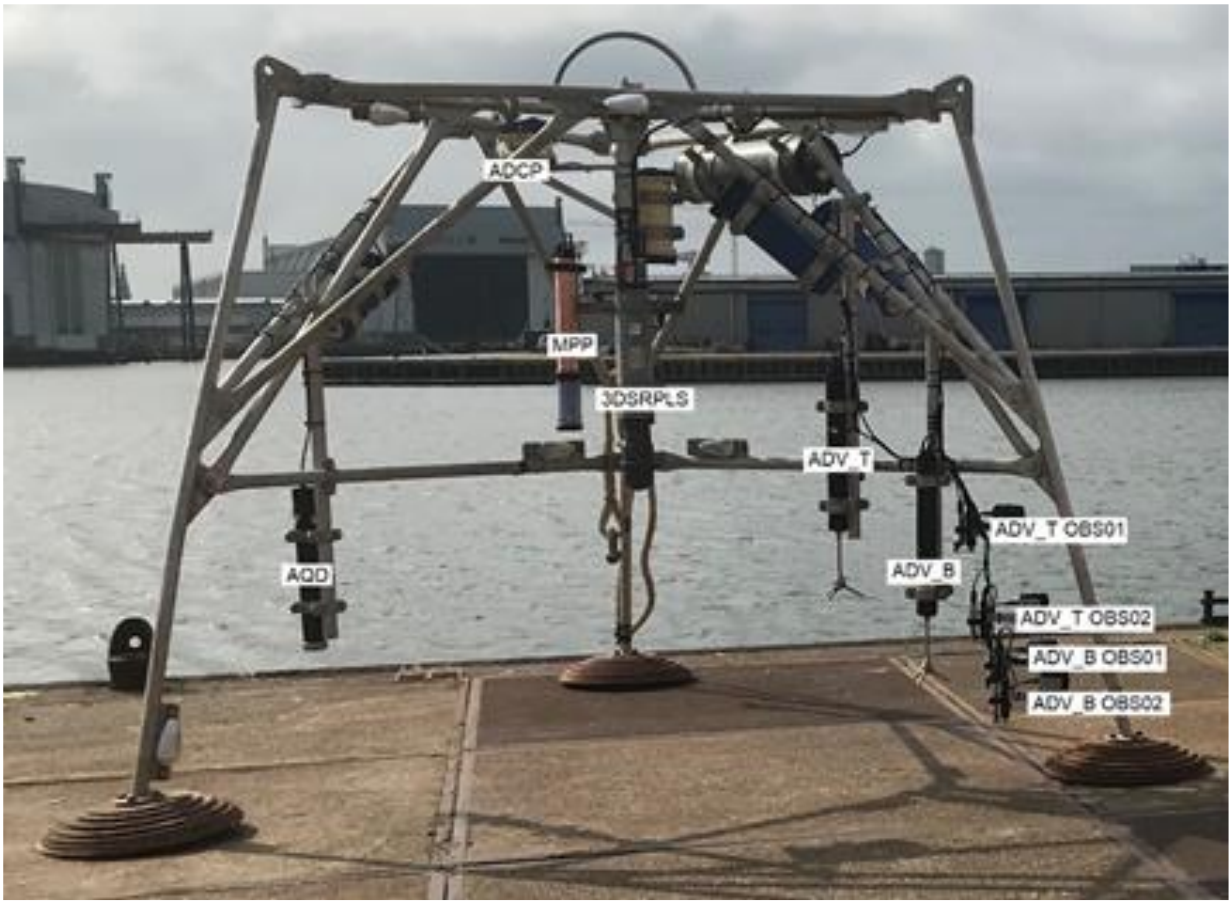

Figure 6: Frame containing all the measuring instruments.

The OBS measures suspended sediment concentration (SSC) in counts. In this study, the OBS signal was converted to sediment concentration with the following formulas and coefficients. The counts are converted to volts

$$Volts = Counts * \frac{5.0}{65535}$$

The signal in volts is then converted to NTU by

$$NTU = \alpha_{volt\_NTU} * Volt^2 + b_{volt\_NTU} * Volt + c_{volt\_NTU}$$

The coefficients used are gained from a calibration curve, which was derived from measuring known NTU values with the OBS sensors. The coefficients for the conversion are found in table 3. The signal is then converted to SSC by

$$SSC = b_{NTU\_SSC} * NTU + c_{NTU\_SSC}$$

The coefficients for the conversion are the same for the four OBS instruments of both F1 and F3 with $b_{NTU\_SSC} = 2.9073$ and $c_{NTU_{SSC}} = 0$. These coefficients were gained with use of sediment samples taken at the measuring location.

The SSC signals calculated for both F1 and F3 contained a few unrealistically high values which were removed.

On July 4th seawater samples were taken around the locations of the two measuring frames. From 08:28 to 09:17 and from 12:01 to 13:17 the samples were taken near F1 from 10:01 to 11:17 and from 14:00 to 15:18 samples were taken near F3. It was low water around 10:50 and peak ebb velocities occurred at 9:00. The SSC was measured, and a distinction was made between sediment larger and smaller than 53 µm. Because there were only a few samples taken near the bed, the pump samples could not be used to further calibrate the OBS signals.

Table 3: Coefficients for the conversion from volt to NTU.

Frame	OBS	a_{volt_NTU}	b_{volt_NTU}	c_{volt_NTU}
F1	OBS_80	1242.3	2312.7	-1.2092
	OBS_50	1113.5	2469.2	-7.2407
	OBS_30	226.53	3425.7	1.1186
	OBS_20	1166.1	2503.2	5.4589
F3	OBS_80	1117.5	2498.3	-8.4508
	OBS_50	1060.3	2442.2	-3.8417
	OBS_30	1071.4	2492.2	-6.4843
	OBS_20	1047.2	2491.2	-4.7516

Wave height, wave direction and wave period are obtained from a wave buoy near the Vlakte van de Raan (figure 4). Wind speed and wind direction are obtained from a measurement station also near the Vlakte van de Raan (figure 4). The cardinal wind direction in degrees is converted to wind speeds going to the east (positive) and to the west (negative) to be able to better compare the wind and the flow velocities. The wind direction is predominantly west-southwest which means the east-west converted wind speeds are a relatively good representation.

3.2 Data analysis

3.2.1 velocity profile

The flow velocities of the AQD, ADCP and ADV's are converted to east-west and north-south components. The flow velocity measurements were averaged over a 10-minute period to gain a time-series of flow velocity measurements. At F3 the east-west component of the flow velocity was used for the velocity profiles because the north-south component was very small. At F1 this was not the case and therefore the total flow velocity was calculated using the Pythagoras theorem. For the sign of the velocity the east-west direction sign was used because this component had the largest influence on the velocity magnitude.

The AQD, ADCP and ADV's measured current velocities were combined to create a vertical flow velocity profile with cell bins of 10 cm for every 10 minutes. The AQD measured flow velocities in the bottom 0.403 meter, the ADV's measured at 0.2 m and 0.5 m and the ADCP from 3.357 m upwards. There are no flow velocity measurements between 0.5 m and 3.357 m.

The lower ADV measured in the same range as the AQD, but not exactly at the same height, and both measurements are used for the profile. The measured velocity magnitude by the ADV was generally slightly lower.

ADCP velocity values at the top of the water column can be distorted due to reflection. Therefore, data less than 0.5 m away from the water surface was not used. The water level time-series was calculated with the pressure data from the ADCP. Brakenhoff et al., (2020) used a logarithmic fit function to create the vertical flow velocity profile, but the measured flow velocities increased or decreased near the top of the water column and a logarithmic function cannot show this change. Therefore, I used a Piecewise Cubic Hermite Interpolating Polynomial (PCHIP) interpolation function through these data points to fit the velocity profile. The fit function created flow velocities every 10 centimetres over the vertical.

With flow velocity values every 10 cm over the vertical, for every 10 minutes of the measuring period, depth averaged flow velocity $\bar{u}(t)$ time-series can be created.

$$\bar{u}(t) = \sum_{i=1}^{h} u_i(t) \Big/ h$$

3.2.2 suspended sediment concentration profile

To find the sediment transport I also need vertical suspended sediment concentration profiles. The SSC measurements contain outliers; therefore, the 10-minute median was taken to create a 10-minute time-series of suspended sediment concentrations. Missing data points are filled in by linear interpolation. The signal of OBS_50 measured from F1 always showed a negative signal and was not used for the profiles while OBS_30 from F3 showed deviating values from the other three OBS instruments and was also not used (figure 7).

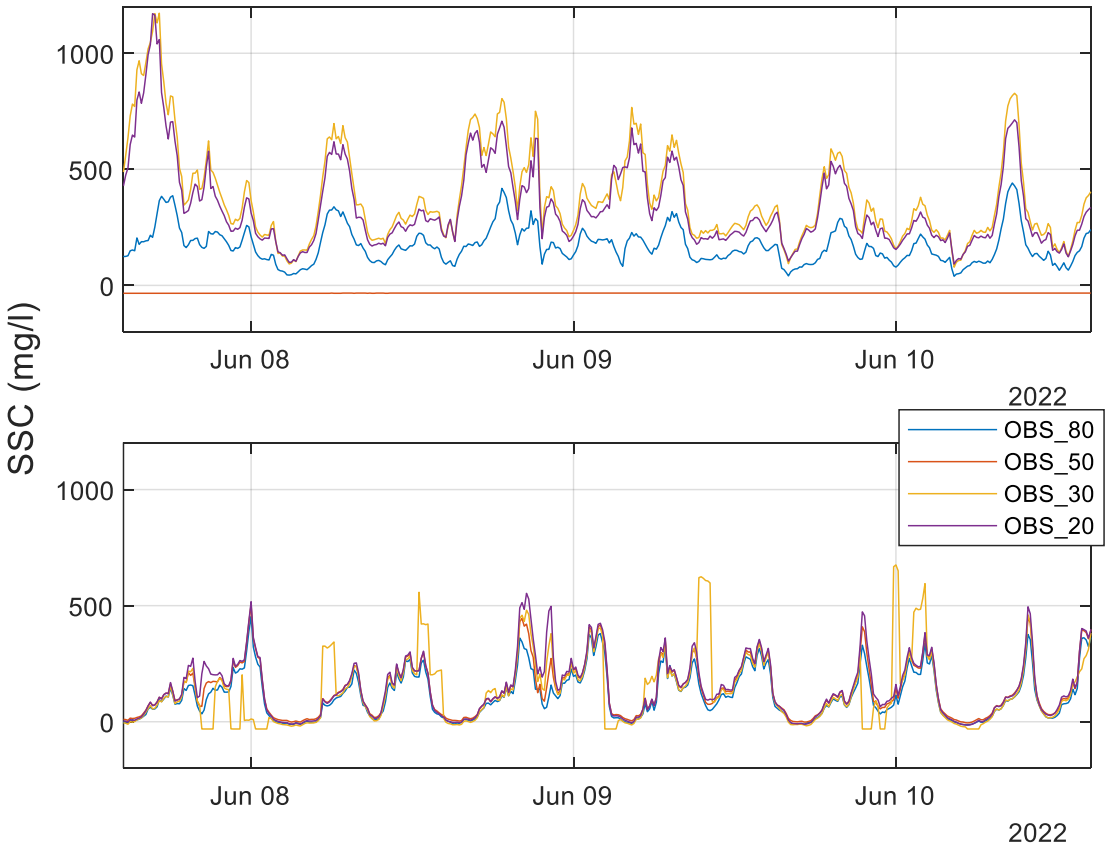

Figure 7: SSC of the four OBS signals for F1 (A) and F3 (B). In A, the signal of OBS_50 is visible which shows a constant negative value and in B the yellow line represents OBS_30 which shows deviating values and pattern from the other three signals.

The profiles are created by a linear line through the data points obtained by the OBS's, with the highest values at the bottom (figure 8, A). SSC cannot become negative, therefore, when the SSC reaches zero, the SSC profile stays zero until the top of the profile. The measured water level time-series is used to determine the top end of the SSC profiles.

When higher located OBS signals measured the highest SSC, the slope of the profile becomes positive, and the SSC will increase with height. This happened mostly in moments of low SSC; therefore, it is unlikely that the SS reached the top of the water column and that the SSC increases with height, and therefore the positive slopes are replaced with the mean slope of the profiles (figure 8, B).

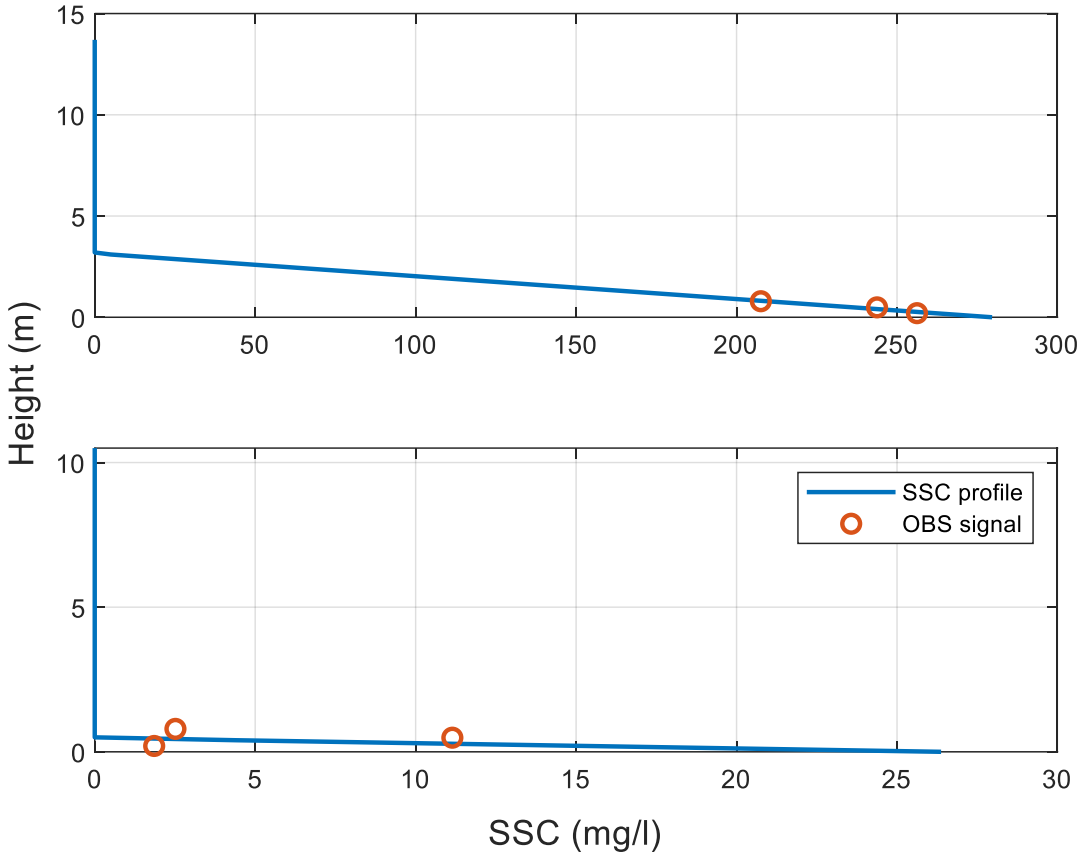

Figure 8: Suspended sediment concentration profiles (blue lines) created from three OBS data points (orange dots), where (A) shows a moment in time where the slope of the profile is negative and the OBS sensor near the bed measures the highest SSC and (B) shows a profile where the positive slope, due to higher SSC measured at the higher OBS sensors, has been replaced by the mean slope.

3.2.3 Tide, currents and SSC characteristics

The duration of the flood and ebb period was calculated by taking the average of the time between low water and high water, and high and low water, for every tidal cycle of the measuring period. The mean peak flow velocity during ebb and flood was calculated by taking the mean of the peaks in depth averaged flow velocity in ebb $\bar{u}_{peak,ebb}$ and flood $\bar{u}_{peak,flood}$ direction. The mean flow velocity for ebb and flood was calculated by taking the mean of the negative $\bar{u}_{ebb}$ and positive $\bar{u}_{flood}$ depth averaged flow velocities, respectively.

The mean SSC during flood and ebb were found by taking the average of the three SSC measurements $\bar{c}$, and splitting the SSC time-series into flood and ebb periods corresponding to moments in time of positive and negative flow velocities. The peak SSC concentrations during ebb $\bar{c}_{p,ebb}$ and flood $\bar{c}_{p,flood}$ were found with the find peaks function in Matlab, with a minimal time difference of 10 hours between the peaks. A 10-hour interval between the peaks was chosen to ensure all peaks were found and also that most of the peaks were the highest peak of that ebb or flood period. The mean of the ebb and flood peaks was taken to calculate mean peak SSC during ebb and flood ($\bar{c}_{m,p,flood}, \bar{c}_{m,p,ebb}$).

3.2.4 Sediment transport and Godin filter

The flow velocity profiles u_{pr} and SSC profiles c_{pr} were multiplied to gain a time-series of sediment transport q_s at every 10 cm over the vertical. The flow velocity and sediment concentration profiles have a time resolution of 10 minutes, so the sediment transport was also calculated per 10 minutes.

$$q_s\,(t) = u_{pr}(t) * c_{pr}\,(t)$$

The depth averaged sediment transport $\overline{q_s}$ was calculated by taking the mean of the sediment transport q_s.

$$\overline{q_s}(t) = mean(q_s\,(t))$$

The sediment transport values q_s (t) were also averaged per meter over the vertical and summed to gain a time-series of the total sediment transport q_{total} over the vertical

$$q_{total}(t) = \sum_{i=1}^{h} \overline{q_s(t)_i}$$

The SSC profiles are most reliable near the bottom, because all three OBS sensors are located there. Higher up in the water column the calculated SSCs might deviate from the actual values because they are an extrapolation from the first meter. Therefore, all sediment transport calculations are done for both near the bed (0 - 1 m) and the whole water column.

The cumulative transport q_{cum} was calculated using the total sediment transport per 10 minutes and multiplying the 10 min average sediment transport values by 600 s. Adding all the values together gives the total cumulative sediment transport. The cumulative sediment transport was also calculated for the bottom meter.

$$q_{cum} = \sum q_{total}(t) * 600$$

The flow velocity u consists of three components: the tidal component u' and two non-tidal components u_{res} and u_a representing residual currents and tidal asymmetry and tidal pumping, respectively.

$$u = u' + u_{res} + u_a$$

A low pass Godin filter was used to remove the tidal variation in the time-series. It filters all tidal components shorter than 30 hours with an efficiency of 99% (Wang et al., 1999). The results of the Godin filter are the non-tidal currents and suspended sediment $< u_i >$ and $< c_i >$ of the flow velocity u_i and the SSC c_i ($< u_i > = u_{res} + u_a$). The non-tidal component $< u_i >$ cannot be split into the residual currents and tidal asymmetry and will further be called the residual current.

The de-tiding was done per meter and only for cells which were always under water and thereby contain a continuous time-series of flow velocities, because the Godin filter does not work properly when there are missing values.

$$< u_i(t) > = Godinfilter\ (u_i(t)), \qquad < c_i(t) > = Godinfilter\ (c_i(t))$$

The residual currents and residual SSCs were multiplied and summed to gain the residual sediment transport.

$$< q_{res}(t) > = \sum_{i=1}^{h_{low\ water}} < u_i(t) > * < c_i(t) >$$

With $h_{low\ water} = 8$ at F1 and $h_{low\ water} = 10$ at F3. The depth averaged residual sediment transport $\overline{< q_{res,i}(t) >}$ was calculated by

$$\overline{< q_{res,i}(t) >} = {< q_{res,i}(t) >}\Big/{h_{low\ water}}$$

By subtracting the residual currents and residual SSC from the original per meter time-series the tidal currents u'_i and tidal SSC c'_i were gained.

$$u'_i(t) = u_i(t) - < u_i(t) >, \quad c'_i(t) = c_i(t) - < c_i(t) >$$

By multiplying these tidal flow velocities and SSCs the sediment transport by tides was calculated. The Godin filter is used on the tidal sediment transport values to calculate the net tidal sediment transport per meter, and by adding these values the total net tidal sediment transport $q_{tide}(t)$ was calculated.

$$< q_{tide}(t) > = \sum_{i=1}^{h_{low\ water}} Godinfilter\ (u'_i(t) * c'_i(t))$$

The depth averaged tidal sediment transport $\overline{< q_{tide}(t) >}$ was calculated by dividing the tidal sediment transport by the depth

$$\overline{< q_{tide}(t) >} = {< q_{tide}(t) >}\Big/{h_{low\ water}}$$

To find the influence of the wind on the surface currents, a Godin filter was used on flow velocities of the surface water layer. The height of the water layer at the surface differs trough time, so for the flow velocities, per moment in time, the highest one-meter cell with flow velocities was used.

$$< u\_surface\ (t) > = Godinfilter\ (u\_surface\ (t))$$

3.2.5 Wave and current bed shear stresses

Wave orbital motions and currents induce bed shear stresses on the bed which can bring the sediment into motion and transport the sediment. To compare the influence of the waves and the currents on the bed shear stress, both the wave induced bed shear stress τ_w and the current induced bed shear stress τ_c are calculated with formulas from Van Der Werf et al. (2022). τ_w is given by

$$\tau_w = \frac{1}{2}\rho_w f_w U_w^2$$

where $\rho_w = 1027$ kg/m^3 is the sea water density, f_w the wave friction factor and U_w the near-bed orbital velocity amplitude. According to Soulsby & Clarke (2005) The wave friction factor f_w is given by

$$f_w = 1.39\left(\frac{A}{z_0}\right)^{-0.52}$$

where $z_0 = k_s/30$ with the roughness height $k_s = 2.5\ D50$ and A is given by

$$A = \frac{U_w T}{2\pi}$$

Where T is the mean wave period.

Asymmetric megaripples and asymmetric or symmetric sand waves are the most frequently observed bed forms in tidal flow conditions, with sand waves occurring in locations with relatively fine sediment (<150 µm)(Van Rijn, 2007). The bed roughness of sand waves is approximately equal to grain/sheet flow roughness (Van Rijn, 2007), while the bed roughness of megaripples is higher. The grain roughness was used for the bed roughness height because the specific bed forms in the location are not known, and with $D50 = 150\ \mu m$, the presence of sand waves is a possibility which would also lead to a grain related bed roughens height.

The median grain-size for both the locations of F1 and F3 is $D50 = 150\ \mu m$. The $D50$ value of $150\ \mu m$ is an estimated mean of the different $D50$ values around the frames. The measured differences in grain size were large over a small distance, so the used value might differ slightly from the actual grain size. But because this grain size is used for the calculations of both the wave and current induced bed shear stresses they can be compared well.

The current related bed shear stress τ_c is calculated using

$$\tau_c = \rho_w f_c u_c^2$$

$$f_c = \left(\frac{\kappa}{\ln\left(\frac{30h}{k_s}\right)}\right)^2$$

Where $\kappa = 0.4$ is the Von Karmann constant, u_c is the depth-averaged velocity and $k_s = 2.5\ D50$ (the same as the wave-related roughness).

The near bed orbital velocity amplitude U_w is determined according to the method which is used in Van Der Werf et al. (2022). First, the ADV_T flow velocity data is de-trended so that the mean of every 10 minutes' equals zero. To filter out velocities with a period longer than 20 s (frequency smaller than 0.05 Hz), a high pass filter was used. The resulting orbital velocity vectors were transformed into time series of total orbital velocity in the direction of wave advance, using eigenfunction analysis (see Ruessink et al., 2012). The resulting orbital velocity signal was smoothed using a moving average window of 3 samples to try and filter out the effect of turbulence. Van Der Werf et al. (2022) smoothed the data by 25 samples because their ADV has a sampling frequency of 16 Hz instead of 2 Hz. The 10-minute mean of

the highest one third of the positive orbital velocity peaks was used to define the significant orbital velocity $u_{mb,1/3}$, which is used as the near bed orbital velocity amplitude U_w.

4. Results

Here I first describe the measured tidal characteristics, tidal currents and SSC and the resulting flow velocity and SSC profiles. Secondly, I show measured wind and waves characteristics and resulting representative bottom orbital velocities and I compare wave and current bed shear stresses. Then I describe the total sediment transport and compare it with the sediment transport near the bed. Finally, the results of the Godin filtered velocities and concentrations are presented together with the residual and tidal sediment transport.

4.1 Tidal characteristics, flow velocity and SSC

The peak depth averaged flow velocity is higher at the location of F3 than at the location of F1 (figure 9). The peak flow velocities differ over the month and follow the spring-neap cycle. The first springtide has a larger water level and velocity amplitude. Positive flow is in Flood direction so flowing to the east and negative velocities are in ebb direction to the west. This is the case for all the tables and figures in this thesis.

The mean duration of the flood period (time from low water to high water) is shorter than the mean duration of the ebb period at both F1 and F3, which corresponds to a flood dominance of the vertical tide (Table 4). Peak flow velocities are higher at F3 than at F1, both during flood and ebb. At F1 the mean peak flood flow velocity is higher than the mean peak ebb flow velocity, corresponding to a flood dominant horizontal asymmetry. At F3 the difference between the peak ebb and flood flow velocities is small but it shows a slight ebb dominant horizontal asymmetry. The mean flow at F1 is almost zero and the mean flow at F3 is larger and directed seaward.

SSC measurements are generally higher at F1 than at F3. The SSC is related to the flow velocity and follows the same spring-neap cycle. The SSC at F3 around June 14th and 15th is lower than the surrounding days and lower than expected looking at the flow velocities.

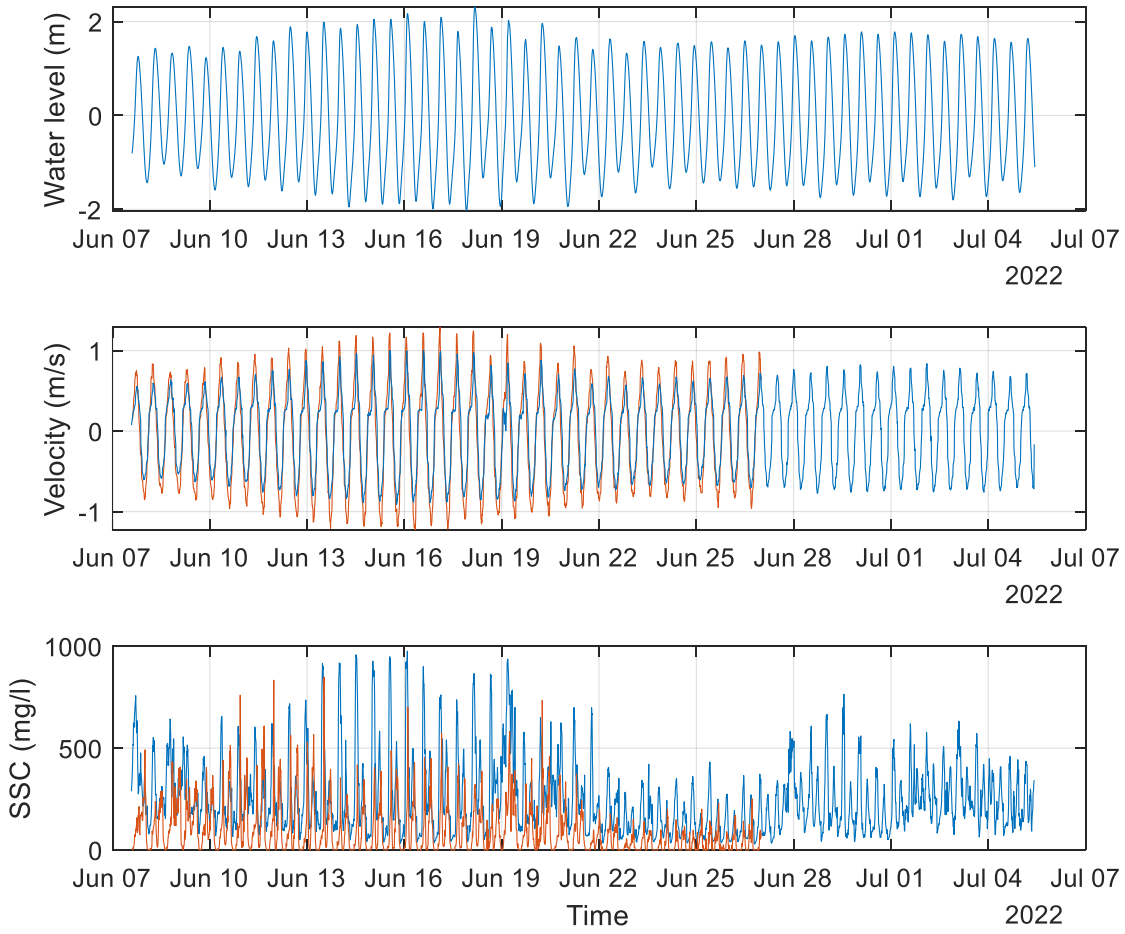

Figure 9: Water level (A), depth averaged flow velocities over the water column (B) and average SSC of the three valid OBS signals (C). The blue line represents the measurements at the location of F1 and the red line the measurements at the location of F3.

Table 4: Characteristics of the tide, tidal currents and SSC at F1 and F3. The first column shows the duration of the ebb and flood period (i.e. the time the currents flow in ebb or flood direction) at both locations, the seconds column shows the time from peak flood flow to peak ebb flow and vice versa, the third column shows the mean peak flow velocities during ebb and flood, the fourth column shows the mean flow, the fifth column shows the duration from peak flow velocity to the peak in SSC, the sixth column shows the peak SSC during ebb and flood and the last column shows the mean SSC during ebb and flood. All the values are an average of the measuring period.

Frame		Duration flood / ebb period (hh:mm:ss)	Time peak flood to peak ebb and vice versa (hh:mm:ss)	Mean peak flow velocity (m/s)	Mean flow (m/s)	Time peak flow to peak SSC (hh:mm:ss)	Peak SSC (mg/l)	Mean SSC (mg/l)
1	Flood	5:53:23	5:10:00	0.76	-0.007	-00:17:02	607.6	282.3
	Ebb	6:32:04	7:15:39	-0.74		00:06:58	381.3	209.9
3	Flood	5:55:39	6:11:37	0.97	-0.06	01:23:41	418.0	100.6
	Ebb	6:29:48	6:15:40	-0.99		00:03:30	393.5	117.4

At F1 the flood flow rises fast but slows down, sometimes for almost 3 hours, before rapidly increasing again (figure 10). The rate at which the velocity increase slows down differs between days. During spring tides this occurs more pronounced than during neap tides. The flow velocities at the location of F3 change more regularly but also show a large increase in velocity before reaching peak flow. The flood flow velocities at F3 reach their maximum about 24 minutes earlier than the flow velocities at F1, while the maximum ebb flow velocities are reached 35 minutes earlier at F1 than at F3. This means that at F1, the time from peak flood flow to peak ebb flow is short (just over 5 hours, table 4), while the time from peak ebb flow to peak flood flow is long (7 hours and 15 minutes). At F3 the time from peak flood flow to peak ebb flow is relatively the same as the time from peak ebb flow to peak flood flow.

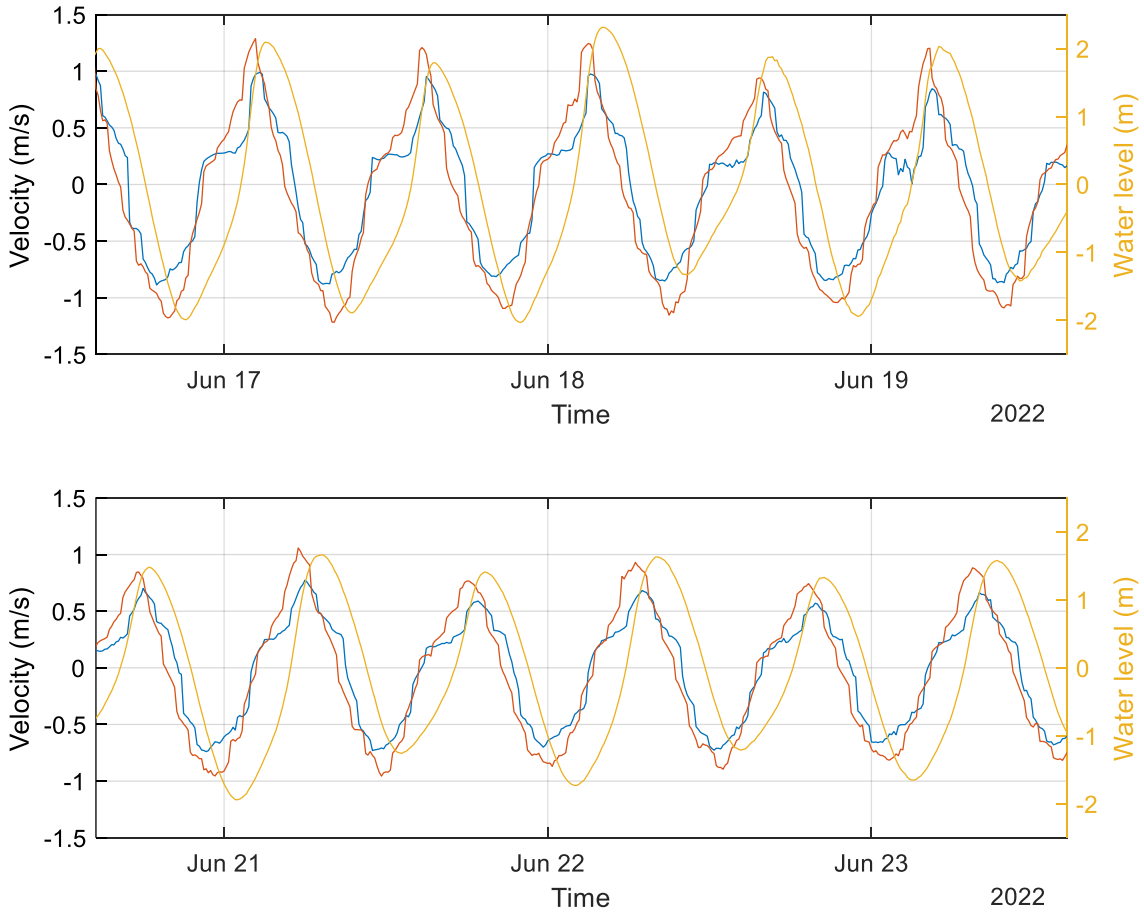

Figure 10: Depth averaged velocity of F1 (red line) and F3 (blue line) and the water level (yellow line).

Peak flow velocities at F1 coincide with peak SSC both during ebb and flood, while at F3 during flood the peak SSC occurs much later than the peak flow (figure 11). At F3, during ebb the mean time from peak flow to peak SSC is about two and a half minutes while during flood SSC peak occurs generally 1 hour and 23 minutes later. At the location of F1 the time from peak flood flow to peak SSC is about 7 minutes and the peak in SSC during ebb occurs about 15 minutes before the peak flow velocity is reached.

At F1, the peak SSC during flood flow is generally higher than the peak SSC during ebb (607 to 381 mg/l, table 4) and the SSCs rise rapidly when the flood flow velocity increases fast. The flood peak of SSC at F3 is also generally higher than the ebb peak (418 to 393 mg/l) but the peak is narrow, and the SSC drops as fast as it rises. This is visible in the mean SSCs during ebb and flood at F3, which is higher during ebb than during flood (table 4). Also, at F1 the SSC almost never reaches zero, while at F3 this happens during most slack-waters. At F1, the SSC at high water slack is generally a bit higher than at low water slack and ranges from 30 mg/l to 100 mg/l. Fine sediment has a longer settling time than coarse sediment, so this could indicate that the suspended sediment at F1 is finer than the sediment at F3.

The late peak in SSC at F3 during flood can cause a net sediment transport in ebb direction, because the high SSCs are not coinciding with the peak flow velocities during flood, while during ebb they do coincide.

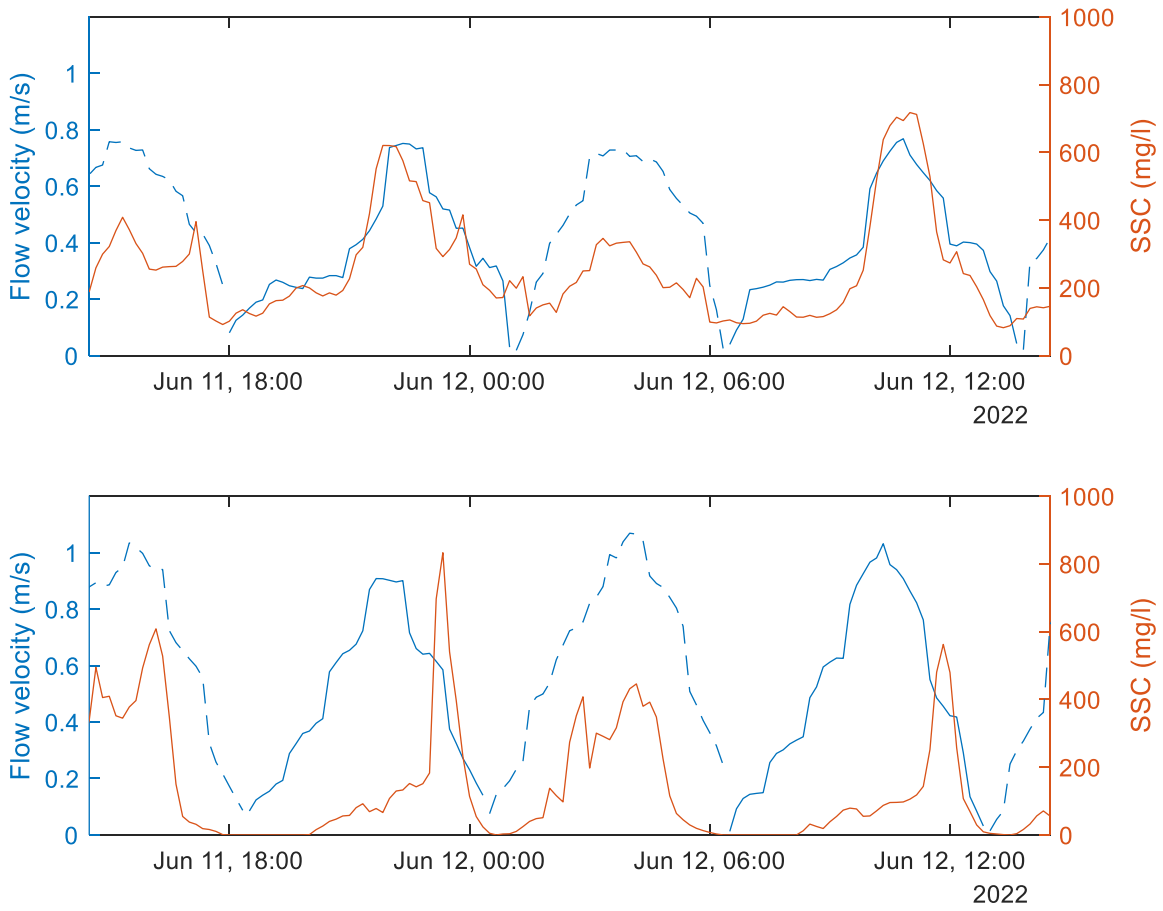

Figure 11: Depth averaged ebb (dashed blue line) and flood (solid blue line) flow velocities (left axis) and averaged SSC (right axis) measured at F1 (A) and F3 (B).

At F1, peak SSCs during flood are reached with smaller flow velocity values than peak SSC during ebb and the peak SSC at ebb is also lower (figure 12). This would suggest that during flood finer sediment is transported, because fine sediment suspends at lower flow velocities.

At F3, during flood, the peaks in flow velocity do not occur at the same time as the peaks in SSC, and peak SSC occurs during times with relatively low flow velocities (figure 11).

A possible explanation for the late SSC peak at F3 could be the sinking of sediment from higher up in the water column after the high flow velocities have passed. But because the concentrations measured with the lowest OBS sensor increase at the same time as the concentrations measured with the highest OBS sensor this is unlikely. A more likely explanation is that the late peak in SSC is caused by fine sediment which gets transported by the tides from a more seaward located area.

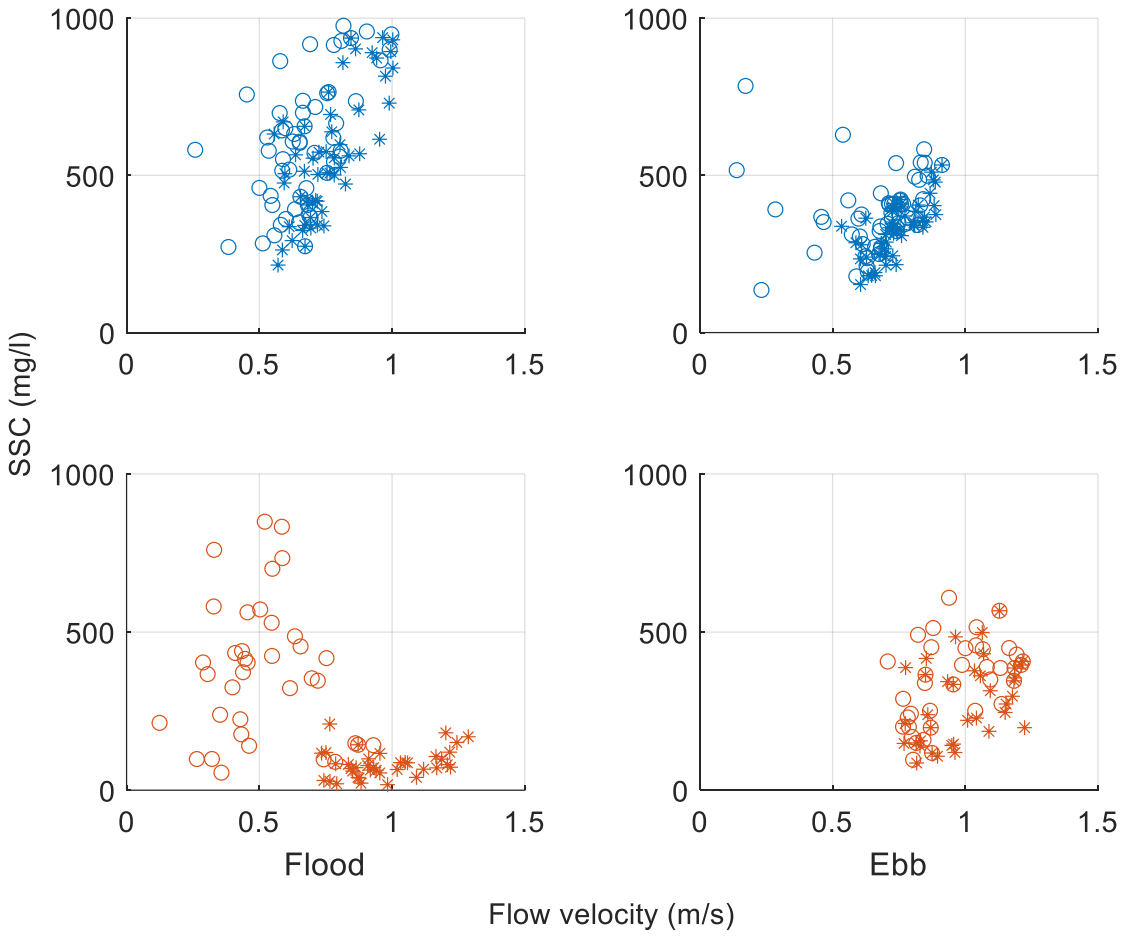

Figure 12: Relation between flow velocities and SSC. The upper graphs (blue) show results at F1 and the lower graphs (orange) show the results at F3. The left Graphs are during flood and the right graphs are during ebb. Circles representing peak sediment concentrations with their respective flow velocity and asterisks representing peak flow velocities with their respective SSC.

The SSC profiles of F1 have larger values near the bottom and lower values near the top of the water column of you compare it with the profiles of F3 (figures 14 & 15). This is because the difference in SSC between the sensor highest in the frame OBS80 and the lower sensors ADV_B_OBS01 and ADV_B_OBS02 is larger at F1 compared to the difference between the SSC signals of the higher placed sensors and the lower hanging sensor in F3 (Figure 7). At F1 and at F3 the mean peak SSC profiles shows larger SSC values than the mean SSC profiles (figures 14 & 15). At F1, the flood SSC profiles contain larger

SSC than the ebb profiles for both the mean and mean peak SSCs. At F3 the SSCs at ebb are higher for both the profiles.

Flow velocities are larger at the location of frame 3 than at frame 1. F3 is in a deeper channel and located more in the channel centre, which results in less friction and thereby higher flow velocities.

The mean ebb flow at F1 is higher than the mean flood flow, while the mean flow over whole measuring period is around zero (figure 14, table 4). This is caused by a longer period of positive flow velocities which are present at F1, while the flow velocity magnitude is lower (figure 11). This contradicts the measured flood and ebb periods at F1, where the time from low water to high water is shorter than the time from high water to low water.

The mean flow velocity magnitude and mean peak flow velocity magnitude at F3 are both larger during ebb. The mean flow velocity profiles during flood and ebb at F3 show a landward increase in flow velocity near the water surface. This can be explained by the mostly westerly wind.

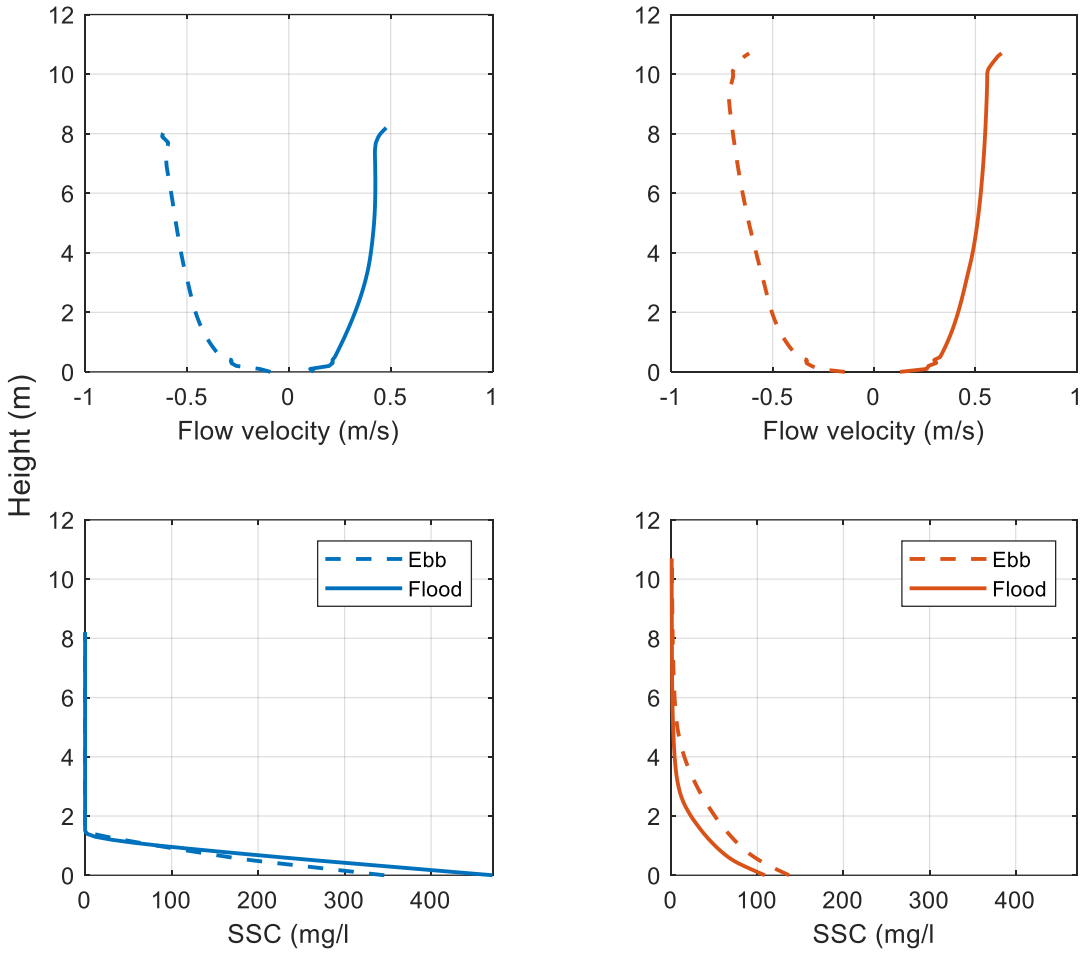

Figure 13: Mean flow velocity profiles (two upper graphs) and mean SSC profiles (two lower graphs), during ebb (dotted line) and flood (solid line) at F1 (blue) and F3 (orange).

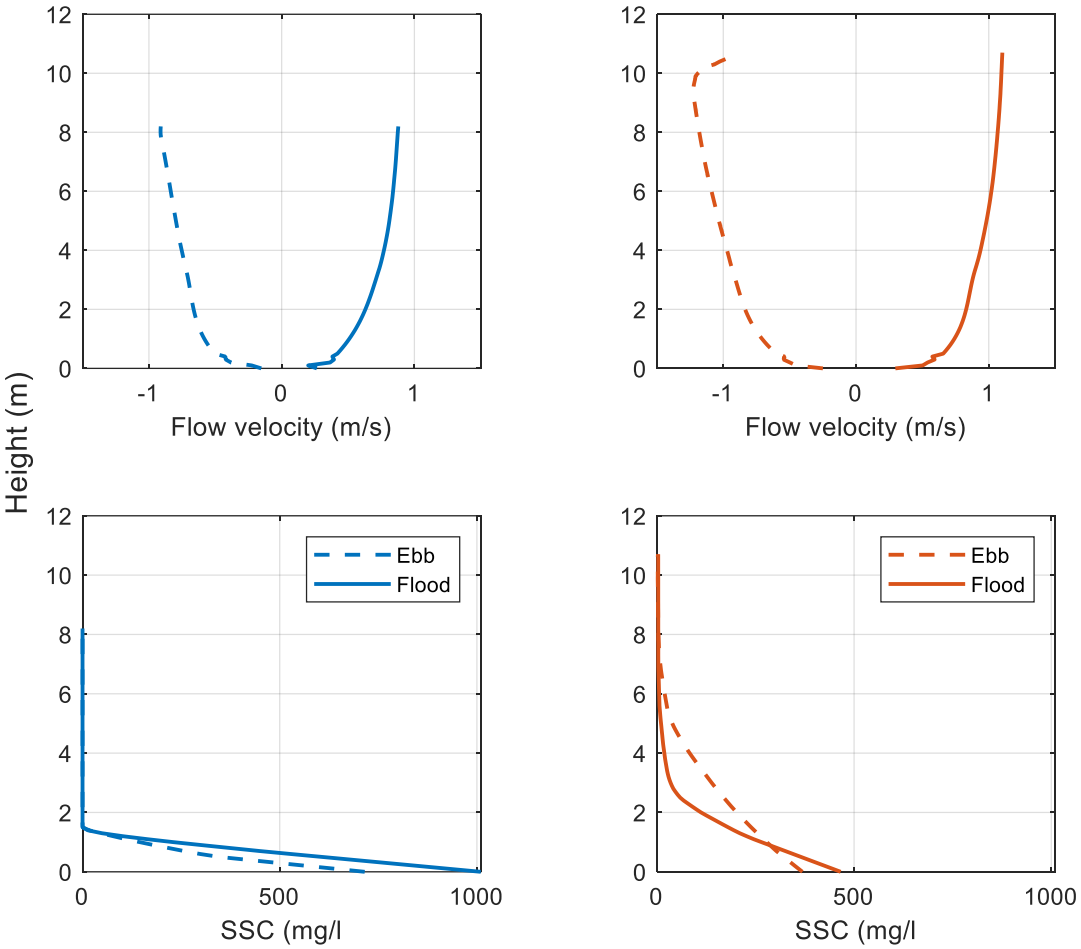

Figure 14: Mean peak flow velocity profiles (two upper graphs) and mean peak SSC profiles (two lower graphs), during ebb (dotted line) and flood (solid line) at F1 (blue) and F3 (orange).

4.2 Wave and wind characteristics and resulting bed shear stresses.

In this section first the wave and wind characteristics during the measuring period are presented. Secondly, the wave orbital motions are visualized. Thirdly, the bed shear stresses induced by waves are presented. These are compared to the bed shear stresses induced by tidal currents, to find out which mechanism causes more transport of sediment.

The wind was predominantly from the west with wind speeds reaching 10 m/s, only between June 12 and June 24 the eastern component of the wind was stronger (figure 16). The significant wave height reached peak wave heights of over 1 meter at around the 9th and 19th of June, corresponding with high wind speeds. Around the 9th the wind came from the west, which is in line with the prevailing wind direction, while on the 19th of June the wind came from the east. Peak wave period varies between 5 and 10 s and the mean wave period stays relatively the same at around 3.5 s. Large peak wave periods do not necessarily coincide with high wave heights.

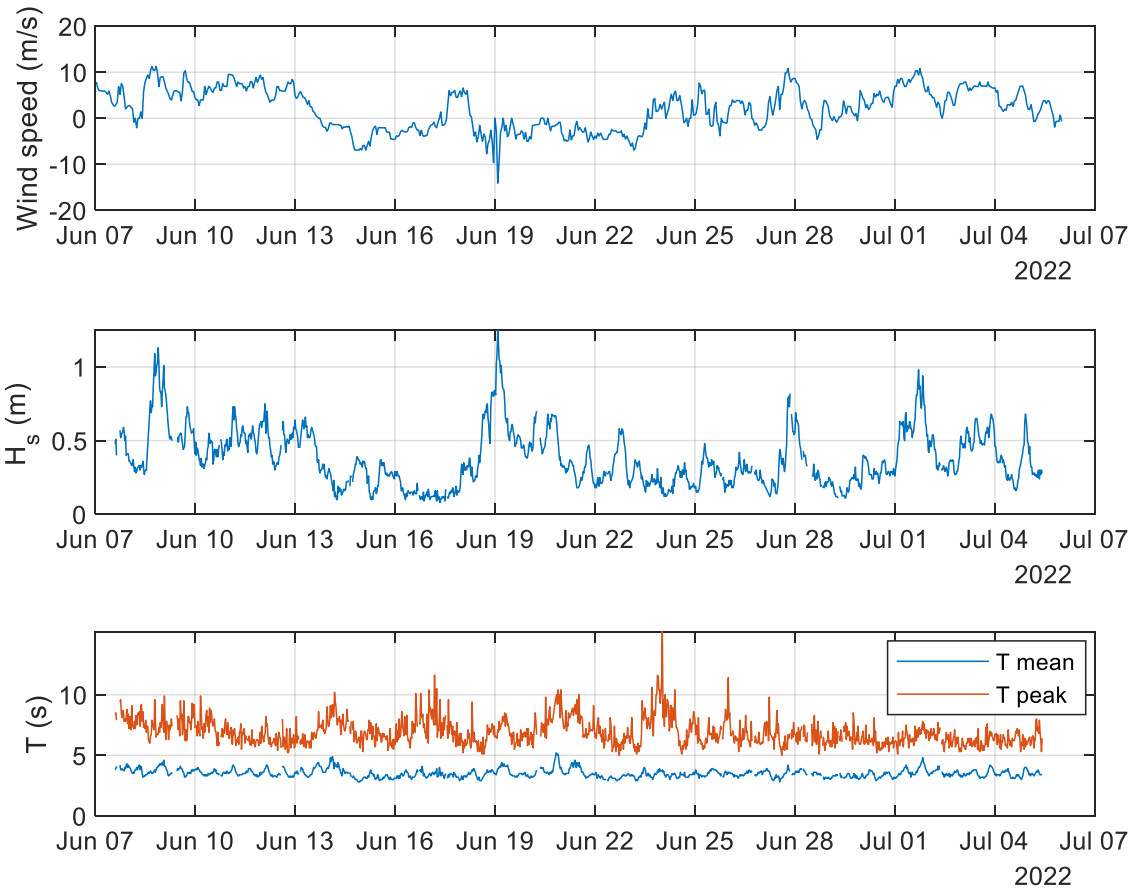

Figure 15: Wind speed in east – west direction (A) with positive values corresponding to winds coming from the west and negative values corresponding to winds coming from the east, significant wave height (B) and mean and peak wave period.

At F1, large wave orbital velocity amplitudes U_w occur during higher wave heights H_s, while at F3, U_w only shows a minor increase during wave events, and highest values are reached during fair weather with high current velocities e.g., around June 16th (figure 17). This suggests the presence of large-scale turbulence which induced flow with the same frequency as the wave orbital motion. The current velocity amplitude at F3 is higher than at F1 because of higher peak flow velocities at F3, both during ebb and during flood.

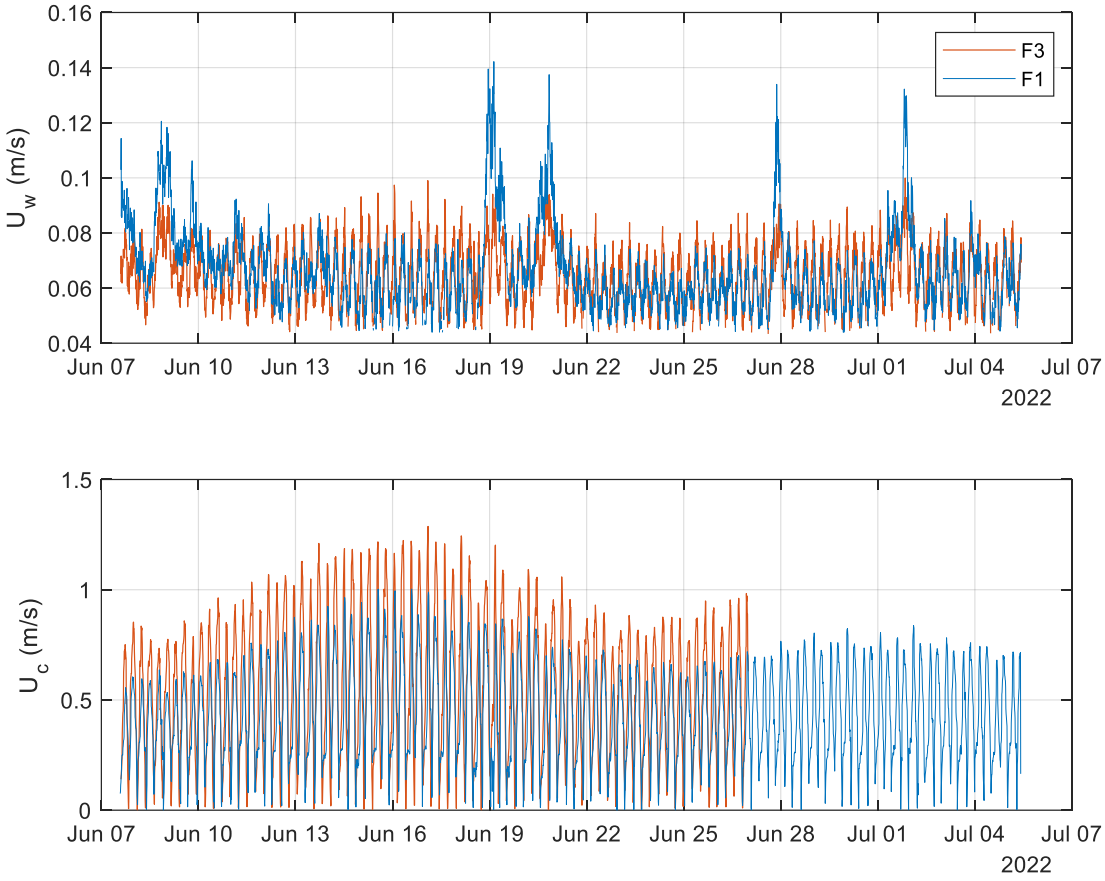

Figure 16: Wave orbital velocity amplitude U_w (A) and current velocity amplitude U_c (B).

The calculated wave induced bed shear stress based on measurements at F3 is generally larger than at F1 and nearly reaches 0.7 N/m^2. Only during the higher wave events on June 8 and June 19 τ_w at F1 exceeded τ_w at F3 (figure 18).

The current induced bed shear stresses (τ_c) at F1 and F3 are much larger than the wave induced bed shear stress reaching respectively 1 N/m^2 and 1.5 N/m^2 during spring tide (figure 18). The current induced bed shear stress at F3 is larger than at F1 because of higher depth averaged current velocities. The higher current induced bed shear stress suggests that the currents are the primary driver of resuspension of sediment at both study locations.

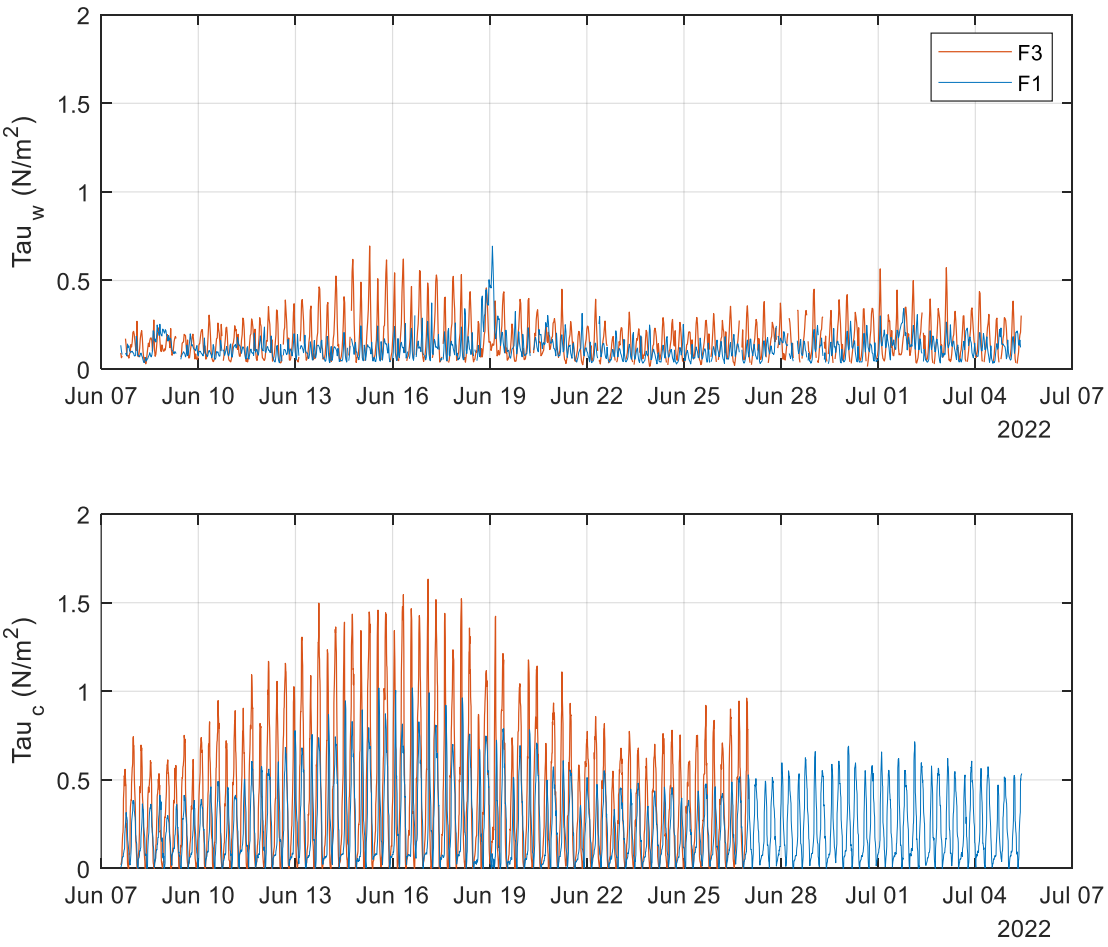

Figure 17: Depth averaged current velocity magnitude (A) and current induced bed shear stresses (B).

4.3 Sediment transport

This section first presents the sediment transport at F1 and F3, calculated near the bed and over the whole vertical (figures 19 and 20). These figures show time-series of sediment transport and their direction and magnitude differences. Lastly, the net sediment transport and its direction and magnitude are visualised.

Sediment transport in the first meter near the bed at F1 shows high values during spring tide, from June 13th to June 19th reaching 800 mg/s/m in positive direction and on other days the transport fluctuates between 200 mg/s/m during peak flood flow velocities and 150 mg/s/m during peak ebb flow velocities. The sediment transport in positive direction is generally larger, except at the end of the measurements. The higher waves present on June 19th caused higher SSCs and consequently more sediment transport in both seaward and landward direction which can be seen in figure 16. On the 23rd of June, an outlier is visible which is caused by a bad SSC measurement of one of the OBS's.

The measurements from F3 show smaller sediment transport values than at F1 in landward direction (positive) but the seaward (negative) sediment transport is higher. Around June 13th the sediment

transport becomes higher, but between the 14th and 16th of June the sediment transport starts to decrease again, opposite to measurements from F1 where the sediment transport is highest in this period.

The sediment transport at locations F1 and F3 show a spring-neap tidal cycle, with more sediment transport at spring tide and less sediment transport during neap tide.

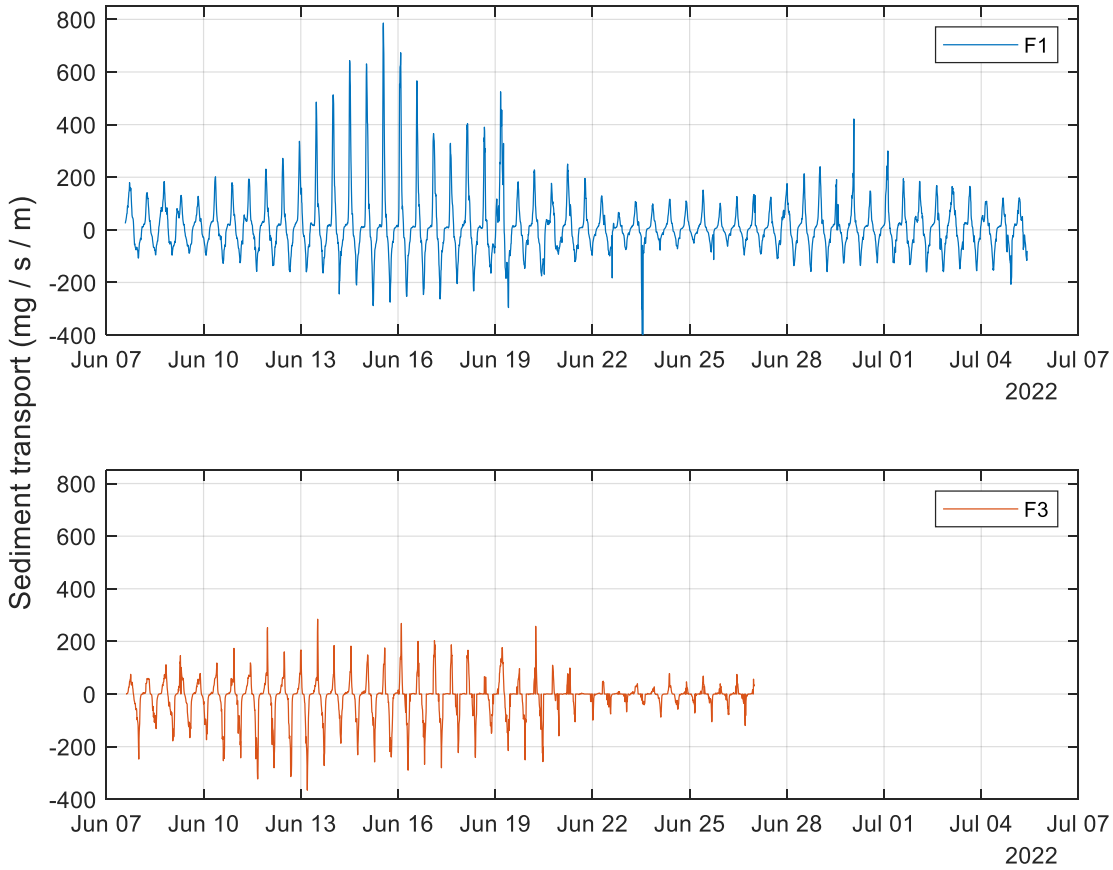

Figure 18: Sediment transport of the first meter from the bed at F1 (A) and F3 (B). The sediment transport follows the spring-neap tidal cycle with higher sediment transport during spring tides and lower sediment transport at neap tide.

The total sediment transport through the whole water column is presented in figure 20. The total sediment transport at F1 shows the same pattern as the sediment transport near the bed, with high positive values from June 13th to June 19th and the wider peak on June 19th is also visible. The same spring-neap cycle is present.

the total sediment transport at F3 has a somewhat the same pattern as the transport near the bed. The total sediment transport at F3 has a few higher peaks than expected when you look at the sediment transport near the bed. These high peaks are caused by the SSC profiles which sometimes contain relatively high SSCs near the top of the water column.This can create large differences between the days.

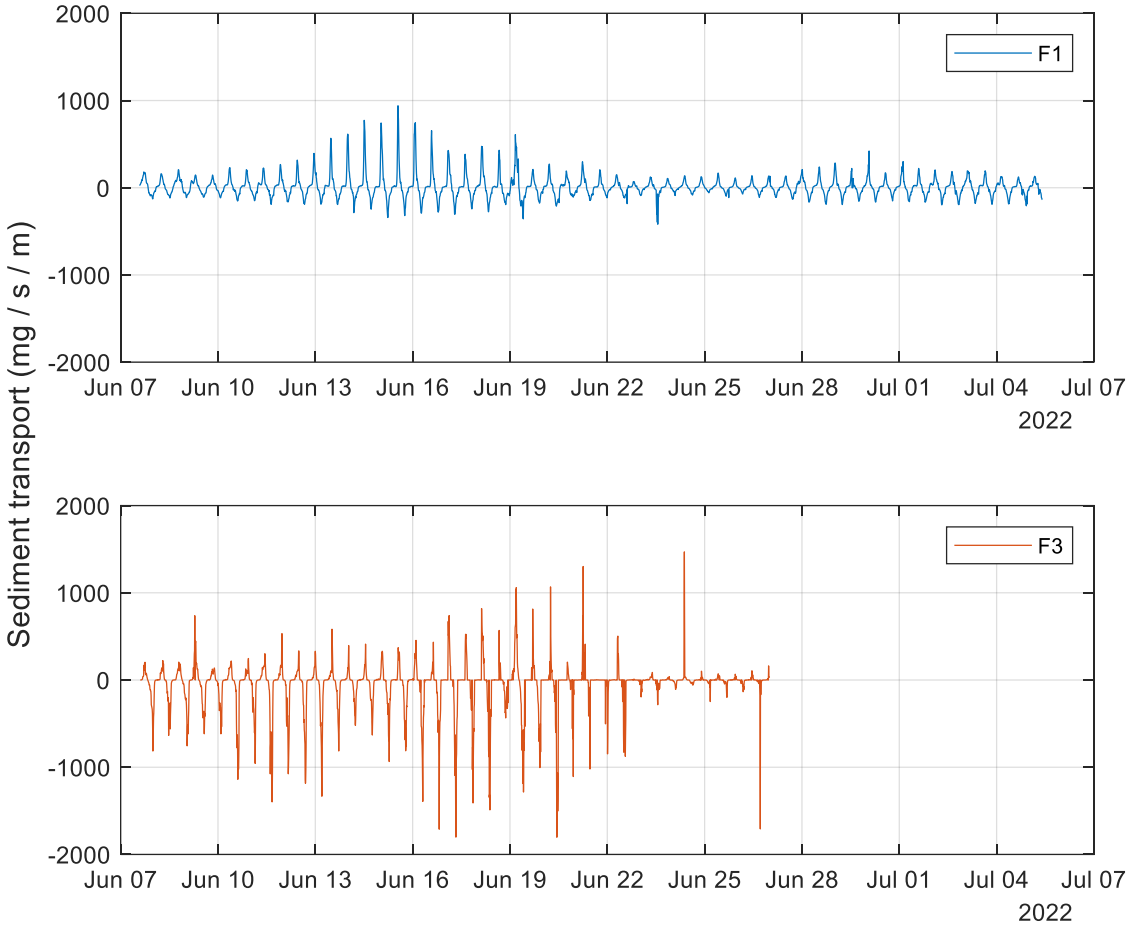

Figure 19: Total sediment transport at F1 (A) and F3 (B).

At the location of F1 the net sediment transport is in landward direction, while at the location of F3 the net sediment transport is in seaward direction (figure 21). Larger fluctuations are visible during spring tide, in moments of higher sediment transport due to high current flow velocities and high sediment concentrations. There are no large sediment transport events visible caused by storms. Only on June 19th you can see a slight increase in sediment transport, especially in the total cumulative sediment transport. But because the higher sediment concentrations were present both during flood and during ebb, the effect on the net sediment transport is small.

The total sediment transported at F1 is 30557 kg/m in flood direction, and the near bed transport was about 29032 kg/m over the course of 1 month. Almost 18000 kg/m was transported during the first spring tide. The total sediment transport at F3 is 86785 kg/m and is seaward directed, while the sediment transport near the bed is only 18507 kg/m.

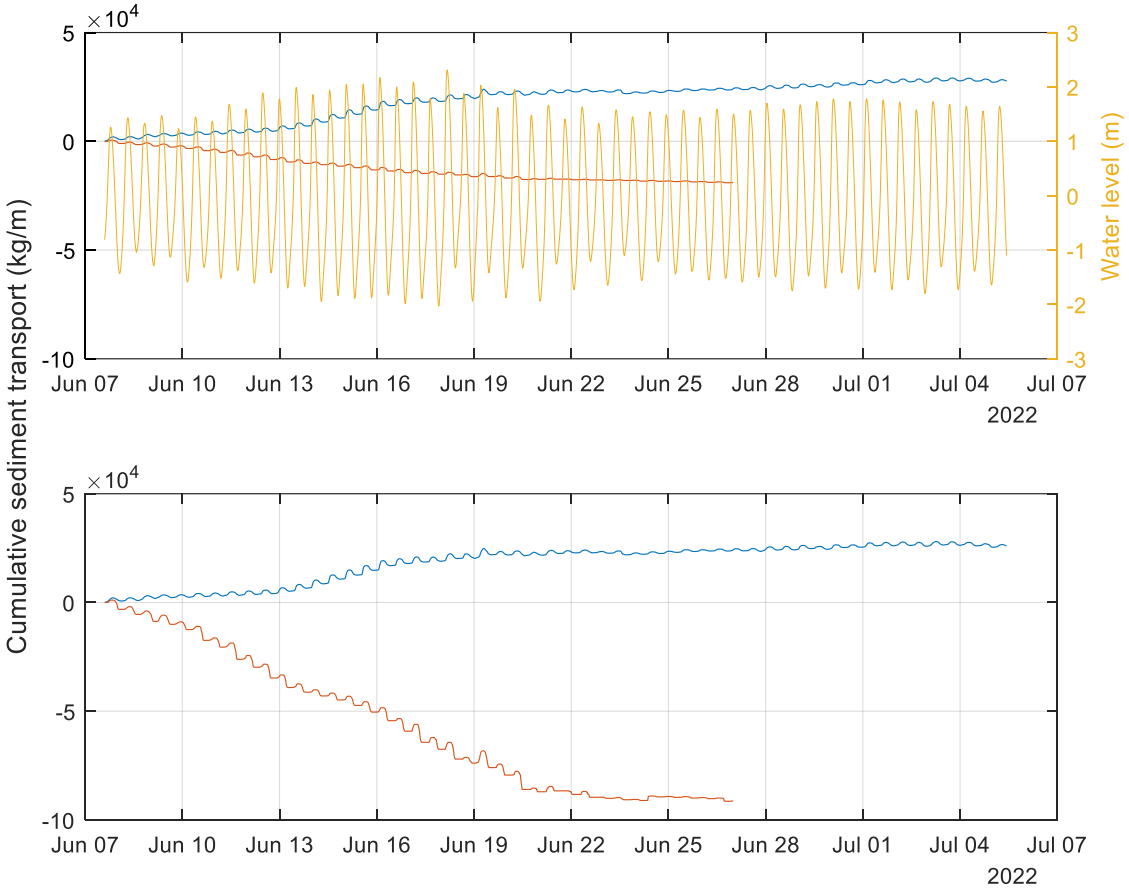

Figure 20: Cumulative sediment transport of the first meter from the bed (A) and the total cumulative sediment transport by the whole water column (B).

4.4 Residual flow & residual and tidal sediment transport

This section presents the net sediment transport by residual currents, tidal asymmetry, and tides. Therefore, firstly the residual depth averaged, surface and near bed currents are presented. Secondly, the residual SSC is presented. Thirdly the tidal components of the currents and SSC are shown and lastly the net sediment transport by residual currents and tidal asymmetry together with the sediment transport by tides is presented.

Higher waves and higher wind speeds coincide with peaks in residual surface currents (figure 22). The residual surface currents at F1 (blue line) show positive peaks on the 9th of June and the 2nd of July, a small peak around the 28th of June and negative peaks at the 15th, 19th and 22nd of June. The direction of the residual surface currents is influenced by the direction of the wind. This is best visible at F1. The first part of the measuring period the wind generally comes from the west which corresponds with positive residual surface currents, until around the 14th of June when the wind direction changes and comes from the east and the residual current direction also changes (figure 22). At around the 24th of June the general wind direction changes again to westerly winds which is also visible in the residual surface current direction. The residual surface currents at F3 are almost always negative but show somewhat the same trend; the same peaks are visible in the signal except for the positive peak around the 9th of June.

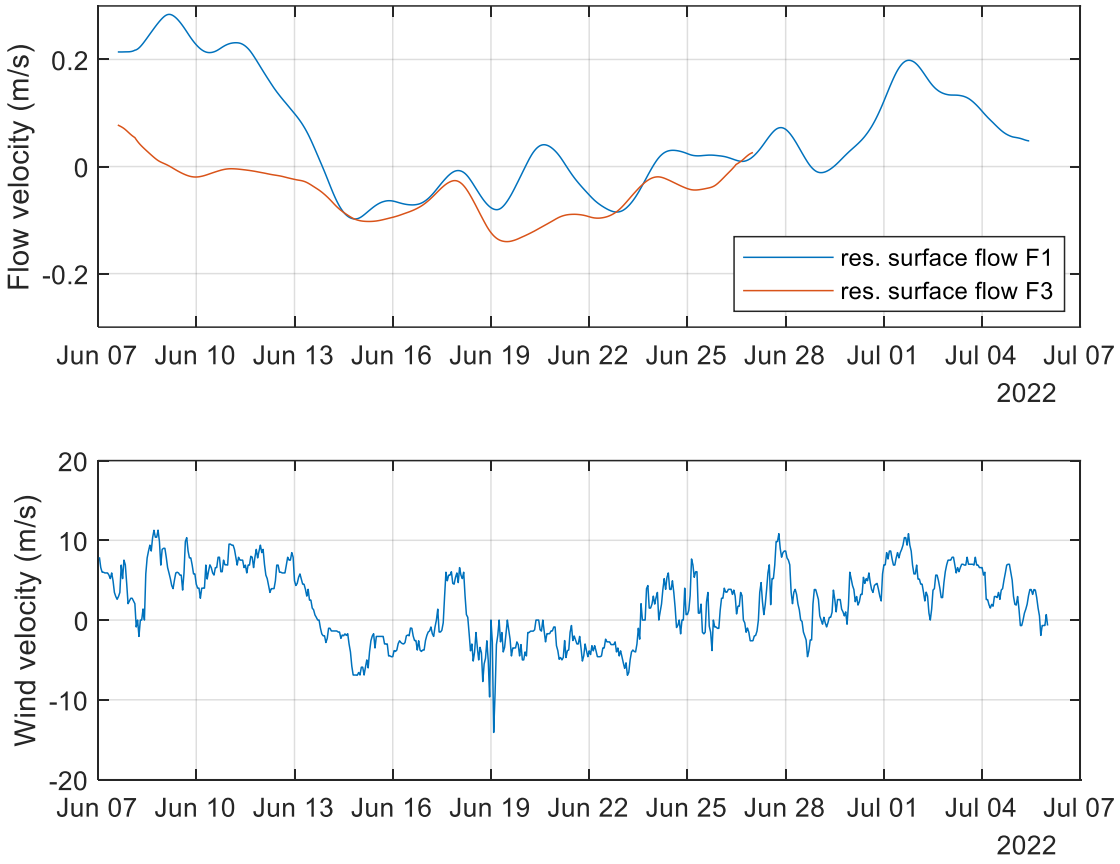

Figure 21: Residual currents at the surface (A) and the wind velocity in east-west direction (B).

The residual currents at the bottom and the depth averaged residual current follow the trends at the surface but are less pronounced at both F1 and F3 (figure 23). The depth averaged residual currents at F1 are almost always negative, while the surface currents were positive at the start and near the end of the measuring period. The residual surface currents reach maximum values of almost 0.25 m/s and -0.067 m/s at F1 and -0.14 m/s at F3, while the depth averaged residual currents only reach 0.043 m/s and -0.052 m/s at F1 and -0.09 m/s at F3. The differences are caused by wind, but also because higher up in the water column the flow velocities are generally higher than near the bed, which create higher residual currents at the surface. Therefore, the depth averaged residual flow velocities are generally higher than the residual flow velocities near the bed at both F1 and F3. Because the residual currents at F1 and F3 are always negative, the wind cannot be the only factor influencing the residual currents.

The residual currents are composed of the residual flow and the tidal asymmetry. Tidal flow in relation with the bathymetry can induce residual flow, which, in a bimodal system, is positive in the flood channels and negative in the ebb channels, as explained in section 1.3.2. Frame 1 is located in a flood channel, and frame 3 is located in an ebb channel, but both channels are part of the larger estuary mouth. Therefore, it is more likely that the system is not truly bimodal and also other mechanism play a role in producing the residual currents. Then, in the relatively shallow parts, the residual flow tends to be in the flood-direction, while in the deeper parts the residual flow is in ebb-direction. Both frames are

located in a channel and would thereby have a residual flow in ebb direction. The mechanism creating the residual currents is most likely a combination of both, because the residual flow is larger in the ebb channel. Another reason for the larger residual currents at F3 is that F3 is located in a deeper channel than F1 ,and thereby flow velocities are higher at F3, creating larger residual currents.

The other component in the non-tidal component of the flow velocity is the tidal asymmetry. Because the total residual currents are seaward while the peak flow velocities at F1 are higher during flood, the horizontal tidal asymmetry is flood dominant at F1. The frames are located not far from each other, and because the vertical tidal asymmetry at both locations is flood dominant, the horizontal tidal asymmetry is also expected to be in flood direction at F3.

Higher waves coincide with peaks in residual SSC e.g., June 19th, June 28th and July 2nd (figure 23). Therefore, the waves have an influence on the residual SSC.

Around June 14th the residual SSC at F3 becomes smaller, while at F1 it becomes more for the depth averaged as the near the bed residual SSC. This results in the lower sediment transport during this period which was mentioned before in section 4.3 and is visible in figures 19 and 20.

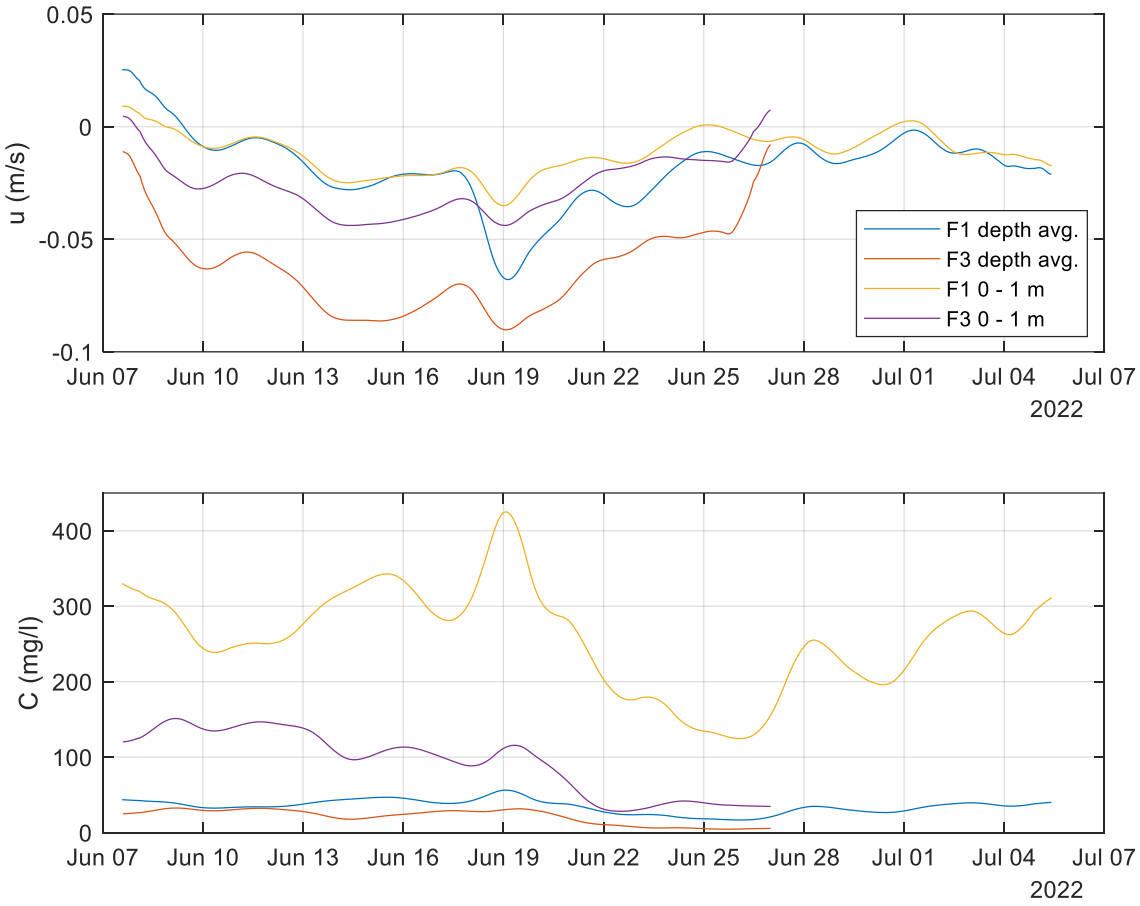

Figure 22: Depth averaged residual flow and residual flow in the first meter from the bed (A) and depth averaged residual SSC and SSC in the first meter from the bed (B). The legend is for both A and B.

The tidal component of the current velocity u' is largest near the surface and smallest near the bed (figure 24) at both F1 and F3. The tidal component of the currents follows the spring-neap cycle and is larger at F3 than at F1.

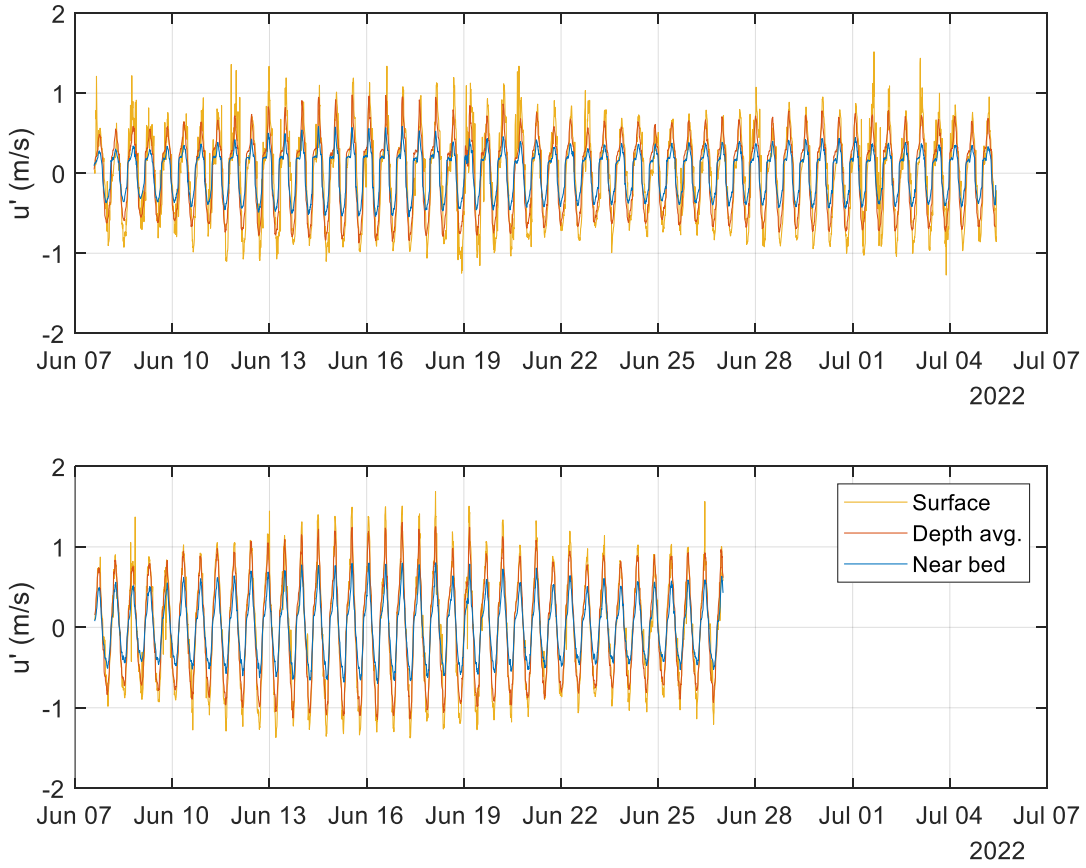

Figure 23: The depth averaged, surface and near bed tidal flow velocity u' at F1 (A) and F3 (B).

The near bed tidally induced SSC c' is larger at F1 than at F3 (figure 25) and the depth averaged tidally induced SSC is about the same at both locations. The trends are similar to the measured SSC at both locations.

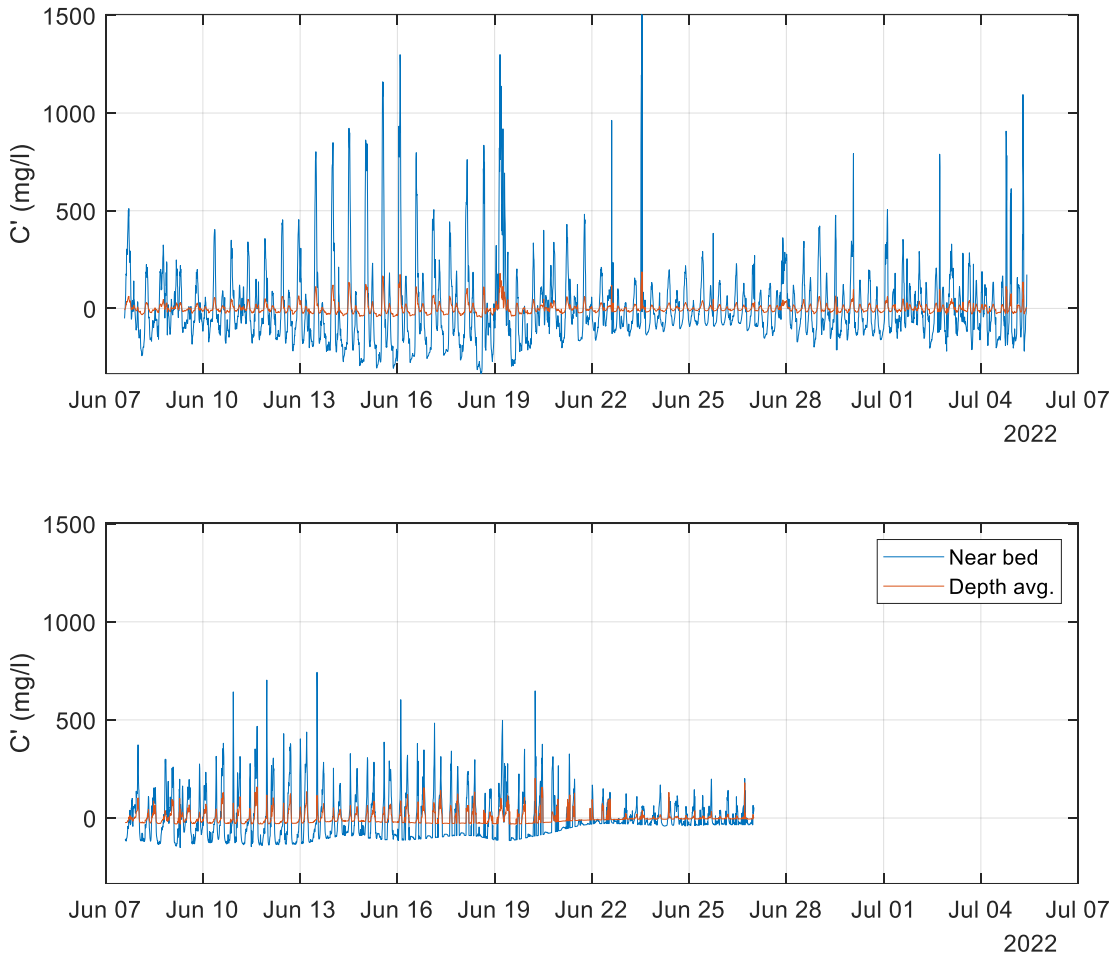

Figure 24: The depth averaged and near bed tidally induced SSC c' at F1 (A) and F3 (B).

The residual sediment transport q_{res} at locations F1 and F3 follows the residual flow velocities present at the locations; at F1 q_{res} is slightly negative in the first week and becomes more negative towards June 14th. The residual sediment transport than shows a large seaward oriented peak around June 19th and fluctuates around zero in the last week of the measurement period. At F3 the residual sediment transport q_{res} is negative for the whole duration of the measurements (figure 25).

The tidal sediment transport is generally positive at F1 and negative at F3 during the measuring period (figure 25). The tidal sediment transport near the bed is higher than the depth averaged tidal sediment transport at both F1 and F3. The tidal sediment transport is larger during spring tide than during neap tide. At F1 the net tidal sediment transport peaks around the 15th of June and is only negative for a short period around June 23rd and at the very end of the measuring period. The tidal sediment transport at F3 peaks earlier around June 12th and shows smaller peaks around June 15th and June 20th which are mostly related to high sediment concentrations at the time.

The tidal sediment transport is larger than the residual sediment transport induced by residual currents and tidal asymmetry. This is especially the case during spring tide, with near bed transport values at F1 reaching 40 mg/s/m and at F3 reaching 22 mg/s/m. The near bed residual sediment transport at F1 shows a large negative peak on June 19th, because of large negative residual flow velocities and large residual SSC. But during the rest of the measuring period the near bed q_{res} does not become more than 7 mg/s/m at F1 and F3.

The net near bed tidal sediment transport is also much larger than the net near bed residual sediment transport (figure 26). At F1, the near bed tidal sediment transport is higher than the actual near bed cumulative sediment transport, because the residual sediment transport is seaward directed and reduces the net landward transport. The tidal component of the sediment transport is more than 4 times larger than the residual component at F1. At F3, both the near bed residual and the near bed tidal sediment transport are seaward directed and combined create a large net seaward sediment transport. At F3, the tidal component is about 3 times larger than the residual sediment transports component.

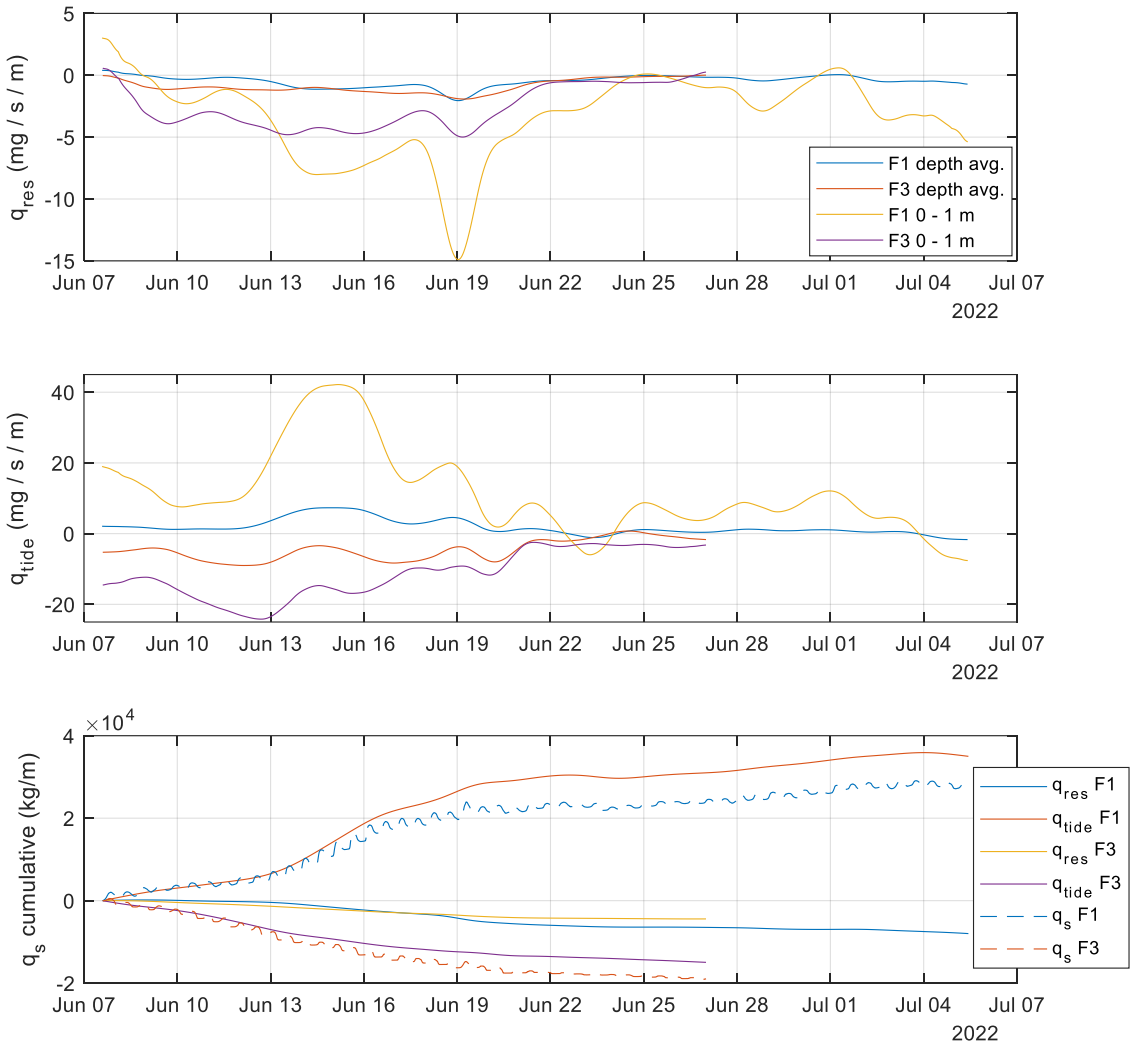

Figure 25: Depth averaged residual sediment transport and residual sediment transport in the first meter from the bed (A), depth averaged tidal sediment transport and tidal sediment transport in the first meter from the bed (B) and the cumulative near bed tidal and residual sediment transport.

The net total tidal sediment transport follows the same trend as the near bid tidal sediment both at F1 and at F3 (figure 27). At F1, the tidal sediment transport is higher than the actual cumulative sediment transport, because the residual sediment transport is seaward directed and reduces the net landward transport. At F3, both the residual and the tidal sediment transport are seaward directed and combined create a large net seaward sediment transport. The total cumulative sediment transport at F3 is larger than at F1.

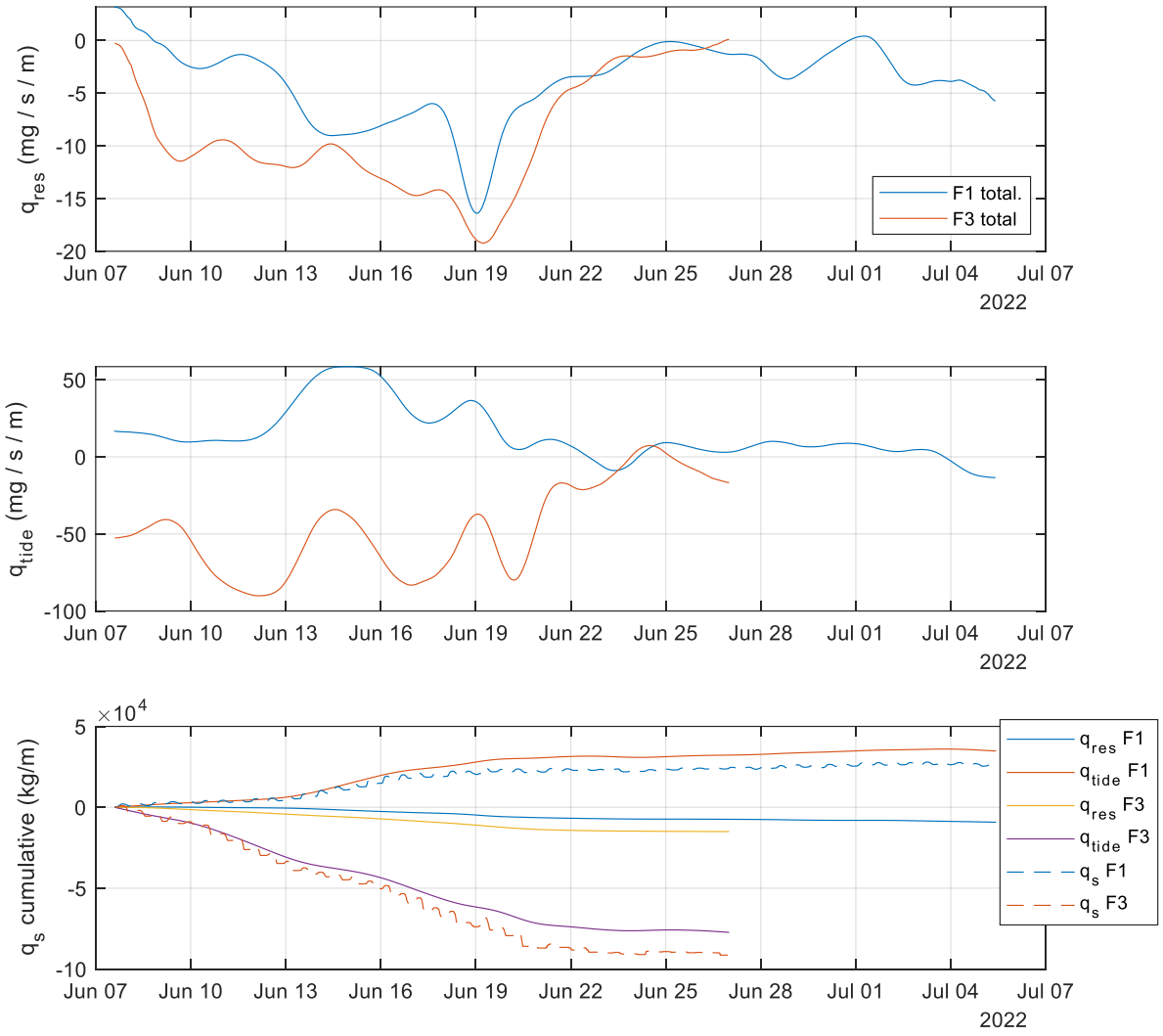

Figure 26: Total tidal sediment transport (A), residual sediment transport (B) and cumulative total tidal and residual sediment transport (C) at F1 and F3.

5. Discussion

In this study I presented the sediment transport and its driving processes for two locations in the mouth of the Western Scheldt. The results showed the influence of the tide, waves, wind, bathymetry and the location on the net sediment transport. In section 5.1 I will discuss potential limitations of my study. In section 5.2 I will discuss interesting results and compare my findings to other studies and in the last section I will discuss the implications of my results.

5.1 Limitations

The SSC values measured at both locations is high when compared to the SSC values gained from the water samples (figure 28). The sampled SSC reached a maximum of 200 mg/l during peak flow velocities

at F3, while the mean peak SSC at F3 is about 400 mg/l (table 4, figure 11). At frame 1 the maximum SSC measured from samples was even lower about 100 mg/l, even though the mean peak SSC at F1 is even higher than at F3. This can partially be explained by the fact that there were no samples taken near F1 in moments of peak flow velocity, but the measured SSC concentrations by the OBS sensors are still higher than from the water samples. OBS sensors are more sensitive to fine sediment and thereby overestimate the presence of fine particles. Therefore, the OBS sensors need to be calibrated via empirical regression models against laboratory or in situ samples, preferably the latter because they provide reference gravimetric concentrations (Fettweis et al., 2019; Gray & Elliot, 2009). But even these calibration models are not always correct, because they are representative of a given flow condition (e.g., calm fair weather with moderate tidal flow) and may be less well suited for high-energy conditions when the sand and mud content can vary strongly in time (Bass et al., 2002). The calibration curve used to convert the volts to NTU values was derived from measuring known NTU values with the OBS sensors. The calibration curve used to convert the NTUs to SSC was obtained with the use of sediment samples taken at the measuring location. This means that the measured SSC values are calibrated relatively well.

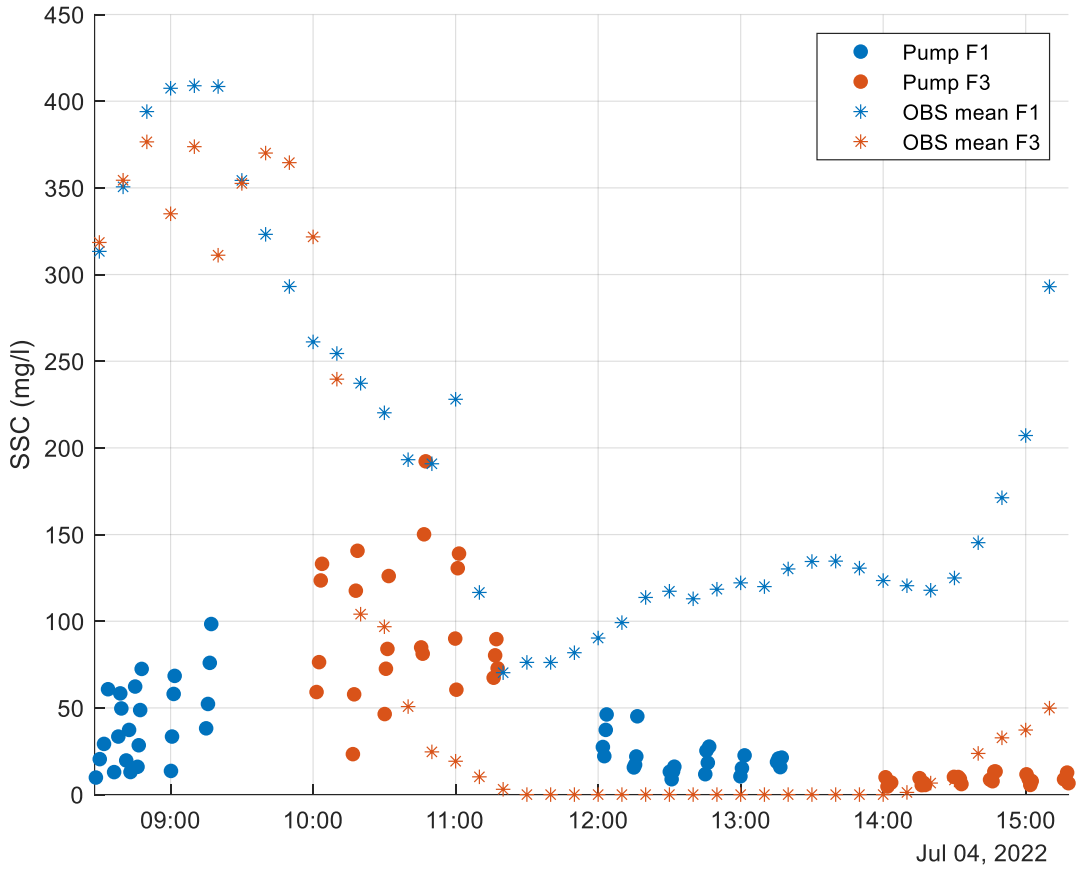

Figure 27: Pump samples taken at the locations of F1 (blue) and F3 (orange) and the mean SSC measured by the OBS sensors.

At F1 the SSC almost never reaches zero, while at F3 this happens after most ebb and flood periods. This could indicate that the suspended sediment at F1 is finer that the sediment at F3. This would also explain the higher SSC measurements at F1, which are not expected because of lower peak flow velocities.

Another explanation for the always present SSC at F1 could be that the OBS sensors had an offset voltage which should have been accounted for (Fugate & Friedrichs, 2002). An argument against this theory is that each OBS has its own specific offset, but all three OBS instruments measure about the same SSCs. Therefore, I went with the first hypothesis and used the values as presented in the result section.

The SSC profiles of F1 and F3 are based on 3 SSCs gained by the three working OBS sensors. The profiles at F1 are all zero above 3 meters, while some profiles at F3 give an SSC value until the top of the water column. The slope of the profile is calculated with a linear line through the three points. At F1 the difference in SSC between the higher located OBS sensor and the lowest sensor is much larger than at F3, which creates a low sloping profile and thus no SSC values after a certain height. At F3 the difference between the SSC values is smaller which creates higher slopes in the profiles. This method is used with the idea that if the concentrations at all three sensors are similar, the sediment is mixed relatively well through the water column, and when the concentrations differ much between the bottom and the top sensor the sediment is less well mixed. But this would suggest that the sediment is finer at F3 because fine sediment remains in suspension longer and has a lower fall velocity (Bass et al., 2007). This is contradictory to what was discussed in the previous paragraph, that the high SSC measurements at F1 might be explained by the presence of finer sediment. Because all three OBS sensors are in the first meter the interpolation of the SSC over the whole water column is less reliable higher up in the water column and the actual SSC values could be different from the predicted. Therefore, all the calculations on sediment transport with the SSC profiles are done for both the first meter from the bed (to gain reliable data, but not the total sediment transport values) and the whole water column (to gain the total sediment transport, although less accurate). The collected pump samples show that around 4 meters from the water surface the SSC is still around 80 mg/l, which would imply that the concentration profiles at F3 which show SSC values higher in the water column are relatively accurate.

In this study I only looked at the east-west components of the flow velocity. At F1 I did use the north-south component to calculate the total flow velocity in the location, but I did not look solely at the north-south component and thereby neglecting possible alongshore currents. The main reason for not taking a closer look at the north-south flow velocities was that the orientation of the flood channel is most likely the cause of the larger north-south component, the flood channel is orientated to the east-northeast. The ebb channel is orientated east-west and has a small north-south component, which would support the hypothesis.

5.2 comparing with other studies.

The SSC values presented in this study are, when compared to the pump samples, most likely higher than the actual SSC in at the mouth of the Western Scheldt. But when comparing the SSC found in the Western Scheldt estuary with findings of (Cook et al., 2007), who studied the sediment transport in the upper Delaware estuary, the near bed SSC has the same order of magnitude. They found near bed SSC between 90 mg/l further up the estuary (Tinicum Island) to 900 mg/l in the middle of the estuary (New Castle), with mean peak current velocities of about 0.9 m/s during ebb. The D50 at New Castle was much smaller than in the western Scheldt, being only 12 µm, and at Tinicum Island it was about 1000 µm. The SSC near the bed (600 mg/l during peak flood at F1 and 400 mg/l at F3) and the suspended sediment D50 (about 65 µm, estimated from the pump samples) in my study area fall well within this range. (Bass et al., 2007) used OBS sensors to present measurements of sand and mud components in the Wash embayment, southern North Sea. Their measured SSC ranges from 200 mg/l to 800 mg/l, with the high values mostly reach during high wave conditions. These values correspond well to the SSC values

presented in my study. Comparing measured SSC values from different estuaries is quite hard, due to different conditions as flow velocities, wave action, sediment availability and sediment type, but this taken into account, the measurements of SSC do correspond relatively well to other studies.

In their study of the Wash embayment (Bass et al., 2007), the peak SSCs during flood were centred around high water slack, which is explained by the transport of mostly muddy material with the flood tide. At F3, the flood SSC peaks also lag behind the peak in flood flow velocity which can thus be explained by higher mud concentrations transported during the flood period. The mud transported near the mouth of the Western Scheldt estuary is about 95% from marine origin (van Kessel et al., 2011). Measurements of SSC near Zeebrugge found tide-averaged suspended particle matter concentrations of about 370 mg/l (van Kessel et al., 2011). This is in line with findings of Chen et al. (2005) who found a marine-dominated muddy estuarine turbidity maximum between Zeebrugge and Vlissingen, with shows suspended matter concentration of more than a few hundred milligram per litre. This area could be the source of the finer sediment which is transported to F3 late in the flood period. The transport of mud during flood is also in line with the findings of Dam & Cleveringa, (2013) who state that the Western Scheldt imports marine mud. During the measuring period, the near bed sediment transport was higher at F1 than at F3, which is the opposite of what would be expected because the current induced bed shear stress is higher at F3 than at F1. This could also indicate that at F1 during flood finer sediment was transported, which is transported by lower flow velocities.

The slack water period, an aspect of the horizontal tidal asymmetry, is not very different at F1 and F3 regarding flow velocities. The flow velocities change from positive to negative (and vice versa) relatively the same in both locations, but the SSC at F1 during slack water is about 30 to 100 mg/l while the SSC at F3 is zero. These values are comparable to the findings of (Cancino & Neves, 1999) who measured the SSC during slack water a bit further up the estuary near Hansweert. the time from peak flood flow to peak ebb flow differs between the two locations. At F1, the time from peak flood to peak ebb flow is short (just over 5 hours), while the time from peak ebb flow to peak flood flow is long (7 hours and 15 minutes). At F3 the time between the peak flow velocities is relatively the same. This can result in more seaward sediment transport, if part of the suspended sediment is still in suspension. The SSC at F1 at the start of the ebb period can thereby be slightly larger than at the start of the flood period, but the effect on net sediment transport is small due to small differences in SSC.

The measured vertical tidal asymmetry at F1 and F3 is flood dominant which is in line with the findings of Wang et al., (2002). The horizontal asymmetry regarding peak flow is flood dominant at F1 with higher peak flow velocities during flood. At F3 the horizontal asymmetry is only slightly ebb dominant with 0.02 m/s higher flow velocities during peak ebb. The horizontal asymmetry at F1 is caused by the M2 + M4 tides and not by residual currents, because the residual currents are negative at F1, while the peak velocities are higher during flood. At F3 the peak flow velocities at ebb and flood are relatively the same, while the residual currents are negative and average about 0.06 m/s. The explanation could be that, at both F1 and F3, the m2 + m4 tides create a tidal asymmetry with higher flood flow velocities, as expected when looking at F1, while a residual flow (e.g., bathymetry induced or wind driven) creates higher ebb flow velocities which create the relatively evenly matched flow velocities. At F1, the residual flow is seaward directed, but the tidal asymmetry has a larger effect and thereby the peak flood flow velocities are larger than the peak ebb flow velocities. At F3, the residual flow is larger and causes the peak ebb flow velocity to be larger than the peak flood flow velocity.

Near the surface, the wind plays a role in creating residual currents. Westerly winds create landward residual currents and easterly winds create seaward residual surface currents. This is clearly visible in the direction of the residual surface currents at F1. This is in line with findings of Bolaños et al. (2013) who state that, in the Dee estuary, the wind is the second most important forcing influencing the residual currents. The residual surface currents can create currents in the deeper parts of the estuary in opposite direction of the main wind direction, driven by a sea level gradient (Gutiérrez de Velasco & Winant, 2004). In the measuring locations, this is not the case, because the near bed residual currents are not in opposite directions of the surface currents, but follow the same trend. This can be explained by the complicated topography of the area, then flow direction varies with depth and is not simply related to the direction of the wind (Gutiérrez de Velasco & Winant, 2004).

The main driving mechanism of the residual currents is most likely tidally induced residual flow due to differences in bathymetry. Frame 1 is located in a flood channel, and frame 3 is located in an ebb channel. In a bimodal system, the residual flow is positive in the flood channels and negative in the ebb channels Wang et al. (1999). But because the channels are part of the larger estuary mouth it is more likely that the system is not truly bimodal and multiple mechanism play a role in producing the residual currents. But the larger underlying theory is that in the relatively shallow parts, the residual flow tends to be in the flood-direction, while in the deeper parts the residual flow is in ebb-direction. Both frames are located in a channel and thereby, the residual currents would be seaward directed. The mechanism creating the residual currents is most likely a combination of both, because the residual flow is larger in the ebb channel than in the flood channel.

The measured wave orbital velocity amplitude presented in this study is comparable to the findings of Van Der Werf et al., (2022). There were no storms during our measurements, but the fair-weather wave orbital velocity amplitudes range in both studies from 0 to 0.2 m/s. They found that with wave heights of 4 meter, the measured orbital velocity amplitude at Ameland, Terschelling and Noordwijk reached about 1 m/s at depths of 12 to 20 m. That would imply that the wave orbital velocity magnitude near the shallower located F1 and F3 could reach values of more than 1 m/s. Unfortunately, because of the absence of high wave events this is not tested. But, because of the sheltering effect of the Vlakte van de Raan, the hypothesis is that the higher waves will most likely break on the shallow shoal and thereby protect the study area from most of the wave energy.

The direction and magnitude of the net sediment transport is mainly determined by the tidal component of the flow velocity (figure 26), with the total sediment transported by the tidal component being more than 4 times than the residual component at F1, and more than 3 times at F3. At F1 and F3, the SSCs were different during ebb and flood which was the cause of the net landward tidal sediment transport at F1 and the net seaward tidal sediment transport at F3. One of the reasons for the differences in SSC during ebb and flood are the peak flow velocities, which were higher during flood at F1, and higher during ebb at F3. The flow velocity magnitude is a combination of different factors; the tidal components, the overtides resulting in tidal asymmetry and the residual currents. The asymmetry of the tides is flood dominant in both locations, and the residual currents are seaward, with larger residual currents at F3, which results in the difference between the ebb and flood peak flow velocities. Waves play a minor role in the sediment transport during the measuring period. Wind is important in creating residual currents near the surface, but because there is less sediment higher up, the influence on the total sediment transport is minor.

5.3 implications

In this study, the sediment transport in two locations at the mouth of the Western Scheldt and tis driving processes are presented. Because of the dynamic nature of the estuary mouth, projecting these findings to other regions is difficult. Nevertheless, this study gives a good insight in the the main sediment transport processes in ebb and flood channels located in a estuary mouth. Thereby, only part of the sediment transport between the sea and the estuary is solved. But with a better understanding of the sediment transport processes, sediment transport models covering larger areas can be improved.

When the two locations are combined, the net near bed sediment transport is landward directed, while the net sediment transport over the whole water column is seaward directed. The seaward total sediment transport can be explained by the method creating the SSC profiles. In further research, to more accurately predict the SSC over the water column, SSC measurements higher up in the water column are needed. Also, more pump samples, both during ebb and flood could give insights in the sediment types transported during ebb and flood.

As for the two locations as potential sediment storage sites; the current induced bed shear stress at F3 is about 1.5 times higher than at F1, thereby, the potential sediment stored will be transported faster by currents at F3 than at F1. The wave induced bed shear stress is higher at F1 than at F3. Although there were no large wave events during the measurement period, the wave orbital velocity magnitude was higher at F1 for the small waves present, and the hypothesis is that during high wave events this will also be the case. During Storms, the sediment at F1 will be transported more, but the magnitude of the transport during high wave events cannot be indicated by this study.

6. Conclusions

The net sediment transport in the two channels near the mouth of the western Scheldt is landward directed in the flood channel and seaward directed in the ebb channel. The total sediment transported at F1 is 30557 kg/m and the near bed transport was about 29032 kg/m over the course of 1 month. Most sediment is transported near the bed, and most sediment transport takes place during spring tides. At F1, during the first spring tide the total near bed sediment transport was about 18000 kg/m. The total sediment transport at F3 is 86785 kg/m, while the sediment transport near the bed is only 18507 kg/m. The direction and magnitude of the net sediment transport is mainly determined by the tidal component of the sediment transport, being four (F1) and tree (F3) times larger than the residual components. At F1 and F3, the SSCs were different during ebb and flood which was the cause of the net landward tidal sediment transport at F1 and the net seaward tidal sediment transport at F3. One of the reasons for the differences in SSC during ebb and flood are the peak flow velocities, which were higher during flood at F1, and higher during ebb at F3. The flow velocity magnitude is a combination of different factors; the tidal components, the overtides resulting in tidal asymmetry and the residual currents. The asymmetry of the tides is flood dominant in both locations, and the residual currents are seaward, with larger residual currents at F3. Due to the large residual currents at F3, the flood dominant tidal asymmetry is opposed and the peak flow velocity are higher during ebb. At F1, the tidal asymmetry is the dominant mechanism and the peak flow velocity during flood is higher.

The main driving mechanism of the residual currents is the tidally induced residual flow due to differences in bathymetry. In a bimodal system, the residual flow is positive in the flood channels and negative in the ebb channels. Because the flood and ebb channel are part of a larger estuary mouth, the system is not truly bimodal, and then in the relatively shallow parts, the residual flow tends to be in the

flood-direction, while in the deeper parts the residual flow is in ebb-direction. The mechanism creating the residual currents is most likely a combination of both, because the residual flow is larger in the ebb channel than in the flood channel. Near the surface, the wind plays a role in creating residual currents. Westerly winds create landward residual currents and easterly winds create seaward residual surface currents. But because the SSCs near the surface are low, the influence of the wind on the net sediment transport is limited.

At F3, the peak SSC during flood is more than 1 hour later than the peak flow velocity which also contributes to the net sediment transport in ebb direction. The late SSC peak is most caused by marine mud which is transported by the flood tides from a more seaward located area, which is in line with other studies stating that the Western Scheldt is a mud importing estuary.

During the measurement period there were no high wave events, therefore, it is difficult to draw conclusion about the role of large wave events on the net sediment transport. The higher waves on June 19 did cause high SSCs, but the resulting extra sediment transport was only slightly visible in the cumulative sediment transport, because the sediment was transported both during flood and ebb. The study site is located in the shelter of the Vlakte van de Raan and thereby, the hypothesis is that the also larger wave events will not be as important as tidal currents and residual currents regarding the net sediment transport.

This study presents the main sediment transport processes in ebb and flood channels located in a estuary mouth. Because of the highly dynamic nature of the estuary mouth, projecting these findings to other regions is difficult. Thereby, only part of the sediment transport between the sea and the estuary is solved. But with a better understanding of the sediment transport processes, sediment transport models covering larger areas can be improved.

7. References

Bass, S. J., Aldridge, J. N., McCave, I. N., & Vincent, C. E. (2002). Phase relationships between fine sediment suspensions and tidal currents in coastal seas. *Journal of Geophysical Research: Oceans*, *107*(C10), 10–11. https://doi.org/10.1029/2001JC001269

Bass, S. J., Mccave, I. N., Rees, J. M., & Vincent, C. E. (2007). *Sand and mud flux estimates using acoustic and optical backscatter sensors: measurements seaward of the Wash, southern North Sea*.

Bolaños, R., Brown, J. M., Amoudry, L. O., & Souza, A. J. (2013). Tidal, riverine, and wind influences on the circulation of a macrotidal estuary. *Journal of Physical Oceanography*, *43*(1), 29–50. https://doi.org/10.1175/JPO-D-11-0156.1

Bolle, A., Bing Wang, Z., Amos, C., & De Ronde, J. (2010). The influence of changes in tidal asymmetry on residual sediment transport in the Western Scheldt. *Continental Shelf Research*, *30*(8), 871–882. https://doi.org/10.1016/J.CSR.2010.03.001

Braat, L., Van Kessel, T., Leuven, J. R. F. W., & Kleinhans, M. G. (2017). Effects of mud supply on large-scale estuary morphology and development over centuries to millennia. *Earth Surface Dynamics*, *5*(4), 617–652. https://doi.org/10.5194/esurf-5-617-2017

Brakenhoff, L., Kleinhans, M., Ruessink, G., & van der Vegt, M. (2020). Spatio-temporal characteristics of small-scale wave–current ripples on the Ameland ebb-tidal delta. *Earth Surface Processes and Landforms*, *45*(5), 1248–1261. https://doi.org/10.1002/esp.4802

Cancino, L., & Neves, R. (1999). Hydrodynamic and sediment suspension modelling in estuarine systems Part II: Application to the Western Scheldt and Gironde estuaries. In *Journal of Marine Systems* (Vol. 22).

Chen, M. S., Wartel, S., Van Eck, B., & Van Maldegem, D. (2005). Suspended matter in the Scheldt estuary. *Hydrobiologia*, *540*(1–3), 79–104. https://doi.org/10.1007/s10750-004-7122-y

Christie, M. C., Dyer, K. R., & Turner, P. (1999). Sediment Flux and Bed Level Measurements from a Macro Tidal Mudflat. *Estuarine, Coastal and Shelf Science*, *49*(5), 667–688. https://doi.org/10.1006/ECSS.1999.0525

Cook, T. L., Sommerfield, C. K., & Wong, K. C. (2007). Observations of tidal and springtime sediment transport in the upper Delaware Estuary. *Estuarine, Coastal and Shelf Science*, *72*(1–2), 235–246. https://doi.org/10.1016/j.ecss.2006.10.014

Dam, G., & Cleveringa, J. (2013). *Grootschalige sedimentbalans van de Westerschelde*. www.imdc.be

Dam, G., van der Wegen, M., Taal, M., & van der Spek, A. (2022). Contrasting behaviour of sand and mud in a long-term sediment budget of the Western Scheldt estuary. *Sedimentology*, *69*(5), 2267–2283. https://doi.org/10.1111/sed.12992

Diaz, M., Grasso, F., Le Hir, P., Sottolichio, A., Caillaud, M., & Thouvenin, B. (2020). Modeling Mud and Sand Transfers Between a Macrotidal Estuary and the Continental Shelf: Influence of the Sediment Transport Parameterization. *Journal of Geophysical Research: Oceans*, *125*(4). https://doi.org/10.1029/2019JC015643

Dyer, K. R. (1997). Partially Mixed and Well-mixed estuaries. *Estuaries: A Physical Introduction*, 146–149. https://www.wiley.com/en-us/Estuaries%3A+A+Physical+Introduction%2C+2nd+Edition-p-9780471974710

Elias, E. P. L., & Hansen, J. E. (2013). Understanding processes controlling sediment transports at the mouth of a highly energetic inlet system (San Francisco Bay, CA). *Marine Geology*, *345*, 207–220. https://doi.org/10.1016/J.MARGEO.2012.07.003

Elias, E. P. L., Jelmer, ;, Ad, C., & Van Der Spek, J. F. (2020). *Large-scale morphological changes and sediment budget 1970-2017 of the Western Scheldt Estuary and Ebb-tidal delta*.

Fettweis, M., Riethmüller, R., Verney, R., Becker, M., Backers, J., Baeye, M., Chapalain, M., Claeys, S., Claus, J., Cox, T., Deloffre, J., Depreiter, D., Druine, F., Flöser, G., Grünler, S., Jourdin, F., Lafite, R., Nauw, J., Nechad, B., … Vereecken, H. (2019). Uncertainties associated with in situ high-frequency long-term observations of suspended particulate matter concentration using optical and acoustic sensors. *Progress in Oceanography*, *178*, 102162. https://doi.org/10.1016/J.POCEAN.2019.102162

Fugate, D. C., & Friedrichs, C. T. (2002). Determining concentration and fall velocity of estuarine particle populations using ADV, OBS and LISST. *Continental Shelf Research*, *22*(11–13), 1867–1886. https://doi.org/10.1016/S0278-4343(02)00043-2

Gray, J. S., & Elliot, M. (2009). Ecology of Marine Sediments: From Science to Management. In *Ecology of marine sediments (2nd ed., 241 pp.). Oxford: Oxford University Press.* https://books.google.nl/books?hl=nl&lr=&id=cIMSDAAAQBAJ&oi=fnd&pg=PR7&dq=Gray,+J.,+%26+Elliott,+M.+(2009).+Ecology+of+marine+sediments+(2nd+ed.,+241+pp.).+Oxford:+Oxford+University+Press&ots=EN0MSfT1ta&sig=qsDC2BGk5Rg5DF7e-3KFrS-Id2E&redir_esc=y#v=onepage

Gutiérrez de Velasco, G., & Winant, C. D. (2004). Wind-and density-driven circulation in a well-mixed inverse estuary. *Journal of Physical Oceanography*, *34*(5), 1103–1116.

Kjerfve, B. (1978). Bathymetry as an indicator of net circulation in well mixed estuaries. In *Limnology and Oceanography* (Vol. 23, Issue 4, pp. 816–821). https://doi.org/10.4319/lo.1978.23.4.0816

Li, C., & O'Donnell, J. (1997). Tidally driven residual circulation in shallow estuaries with lateral depth variation. *Journal of Geophysical Research: Oceans*, *102*(C13), 27915–27929. https://doi.org/10.1029/97JC02330

Mengual, B., Bertin, X., Place, F., Pezerat, M., Coulombier, T., Mendes, D., & Fortunato, A. B. (2022). Wave-current interactions at the Tagus Estuary Mouth (Portugal) under storm wave conditions. *Ocean Modelling*, *175*, 102035. https://doi.org/10.1016/J.OCEMOD.2022.102035

Nayak, A. R., Li, C., Kiani, B. T., & Katz, J. (2015). On the wave and current interaction with a rippled seabed in the coastal ocean bottom boundary layer. *Journal of Geophysical Research: Oceans*, *120*(7), 4595–4624. https://doi.org/10.1002/2014JC010606

Ridderinkhof, H. (1988a). Tidal and residual flows in the Western Dutch Wadden Sea I: Numerical model results. *Netherlands Journal of Sea Research*, *22*(1), 1–21. https://doi.org/10.1016/0077-7579(88)90049-X

Ridderinkhof, H. (1988b). Tidal and residual flows in the western Dutch Wadden Sea II: An analytical model to study the constant flow between connected tidal basins. *Netherlands Journal of Sea Research*, *22*(3), 185–198. https://doi.org/10.1016/0077-7579(88)90022-1

Ridderinkhof, H. (1989). Tidal and residual flows in the western Dutch Wadden Sea III: Vorticity balances. *Netherlands Journal of Sea Research*, *24*(1), 9–26. https://doi.org/10.1016/0077-7579(89)90166-X

Roskam, A. P. (1988). *Golfklimaten voor de Nederlandse kust*. Rijkswaterstaat, Dienst Getijdewateren.

Ruessink, B. G., Ramaekers, G., & Van Rijn, L. C. (2012). *On the parameterization of the free-stream non-linear wave orbital motion in nearshore morphodynamic models*. https://doi.org/10.1016/j.coastaleng.2012.03.006

Santermans, J. (2013). *Achtergrondrapport Baggeren en Storten. Analyse van sediment-eigenschappen, baggerstatistiek, stortintensiteitskaarten en zandwinning in de Wester- en Beneden-Zeeschelde.*

Shellenbarger, G. G., Wright, S. A., & Schoellhamer, D. H. (2013). A sediment budget for the southern reach in San Francisco Bay, CA: Implications for habitat restoration. *Marine Geology*, *345*, 281–293. https://doi.org/10.1016/J.MARGEO.2013.05.007

Soulsby, R. L., & Clarke, S. (2005). *Bed Shear-stresses Under Combined Waves and Currents on Smooth and Rough Beds Produced within Defra project FD1905 (EstProc)*.

Van Der Werf, J. J., Schrijvershof, R. A., Brakenhoff, L. B., & Grasmeijer, B. T. (2022). *Observations of near-bed orbital velocities and small-scale bedforms on the Dutch lower shoreface*. https://doi.org/10.1016/j.ocecoaman.2021.106012

van Kessel, T., Vanlede, J., & de Kok, J. (2011). Development of a mud transport model for the Scheldt estuary. *Continental Shelf Research*, *31*(10 SUPPL.). https://doi.org/10.1016/j.csr.2010.12.006

Van Rijn, L. C. (2007). Unified View of Sediment Transport by Currents and Waves. I: Initiation of Motion, Bed Roughness, and Bed-Load Transport. *Journal of Hydraulic Engineering*, *133*(6). https://doi.org/10.1061/ASCE0733-94292007133:6649

van Veen, J. (1950). Eb- en vloedschaar systemen in de Nederlandse Getijdewateren. *Tijdschrift KNAG*, *67*(2), 303–325.

Verlaan, P. A. J. (1998). Mixing of marine and fluvial particles in the Scheldt estuary. *Ph.D. Thesis, Delft University of Technology, the Netherlands*.

Wang, Z. B., Jeuken, C., & De Vriend, H. J. (1999). *Tidal asymmetry and residual sediment transport in estuaries A literature study and application to the W estern Scheldt WL I delft hydraulics*.

Wang, Z. B., Jeuken, M. C. J. L., Gerritsen, H., De Vriend, H. J., & Kornman, B. A. (2002). Morphology and asymmetry of the vertical tide in the Westerschelde estuary. *Continental Shelf Research*, *22*(17), 2599–2609. https://doi.org/10.1016/S0278-4343(02)00134-6

Wartel, s. (1977). Composition, transport and origin of sediments in the Schelde estuary. *Geol. Mijnbouw*, *56*, 219–233.

Wijnberg, K. M., Nederlands, K., & Genootschap, A. (1995). *Morphologic behaviour of a barred coast over a period of decades*. Koninklijk Nederlands Aardrijkskundig Genootschap (KNAG). https://research.utwente.nl/en/publications/morphologic-behaviour-of-a-barred-coast-over-a-period-of-decades

Zimmerman J. (1980). Vorticity transfer by tidal currents over an irregular topography. *J. Mar. Res.*, *38*, 601–630. https://cir.nii.ac.jp/crid/1572543026342453376

Zimmerman, J. T. F. (1978). Topographic generation of residual circulation by oscillatory (tidal) currents. *Geophysical & Astrophysical Fluid Dynamics*, *11*(1), 35–47. https://doi.org/10.1080/03091927808242650

Zimmerman, J. T. F. (1981). Dynamics, diffusion and geomorphological significance of tidal residual eddies. *Nature*, *290*(5807), 549–555. https://doi.org/10.1038/290549a0